Norwegian University
of Life Sciences

Master's Thesis 2023 30 ECTS
Faculty of Chemistry, Biotechnology and Food Sciences

Identification of Specific N-Acyl-L-Homoserine Lactones by Use of Direct Infusion ESI-MS

Live Solhaug
Integrated Master's Degree in Chemistry and Biotechnology

Abstract

Gram-negative bacteria make up a large portion of life on earth. An understanding of their methods of communication is necessary for our full understanding of their behaviours. With a deeper insight into their methods of communication, we can further our understanding of when and why they perform certain behaviours, such as biofilm production, and further learn to speak their language. These bacteria communicate through a process known as quorum sensing.

A group of Quorum Sensing Signalling Molecules (QSSMs) was studied in this project; N-acyl-L-homoserine lactones (AHLs). QSSMs are molecules of low molecular weight (100 to ~300 amu) employed by bacteria for intercellular communication to coordinate functional behaviour such as biofilm development and secondary metabolite production.

A method of identification of six AHLs using direct infusion electrospray ionisation mass spectrometry was established. Using several known product ions representing the different AHLs established from collision-induced dissociation analysis performed on known amounts of the six AHLs and applying the theory to a solution containing all six AHLs, one can furthermore identify their presence in any kind of solution. The method that was developed, though capable of analysing multiple analytes, is time consuming to use. Manual interpretation of the spectra is necessary. Finding the diagnostic peaks for each analyte was also completed manually.

An attempt was made to create a method for quantification of the same AHLs using a standard curve dependent on the abundance of detected $[M+H]^+$ and $[M+Na]^+$ ions, however this part of the project was discontinued. The partially developed method did not yield useful results.

The methods proved to be time consuming, and other options such as using an autosampler, using internal standards and coupling the MS with an HPLC instrument could greatly reduce the time spent developing and using a method of quantification.

Sammendrag

Gram-negative bakterier utgjør en stor andel av livet på jorda. En forståelse av deres kommunikasjonsmetoder er nødvendig for vår forståelse av deres oppførsel. Med dypere innsikt i kommunikasjonsmetodene deres kan vi styrke vår forståelse av når og hvorfor de utfører forskjellige atferder, slik som biofilmproduksjon, og videre lære oss språket deres. Disse bakteriene kommuniserer gjennom en prosess kjent som quorum sansing.

En gruppe quorum sansende signalmolekyler (QSSMer) ble studert i dette prosjektet: N-acyl-L-homoserine laktoner (AHLer). QSSMer er molekyler med lav molekylvekt (100 til ~ 300 amu) som brukes av bakterier for intercellulær kommunikasjon for å koordinere atferd slik som biofilmproduksjon og sekundær metabolittproduksjon.

En identifikasjonsmetode for seks AHLer ved bruk av direct infusion electrospray ionisation mass spectrometry ble etablert. Ved bruk av kjente produktioner som oppsto fra ionisering av AHLer med bruk av collision-induced dissociation analyse på kjente mengder av de seks AHLene kan en finne ut om de er til stede i andre løsninger. Metoden som ble utviklet, selv om den kan brukes til analyse av mange analytter, er tidkrevende å bruke. Manuell tolkning av spektre er nødvendig, både for å finne diagnostiske topper og for å senere tolke resultatene fra en prøve.

Det ble forsøkt å lage en metode for kvantifisering av de samme AHLene med bruk av en standardkurve avhengig av mengden detekterte $[M+H]^+$ og $[M+Na]^+$ ioner, men denne delen av prosjektet ble forlatt da prosjektets størrelse ble redusert. Den delvis utviklede metoden ga ikke brukbare resultater.

Metodene viste seg å være tidkrevende, og andre alternativer slik som bruk av autosampler, internstandard og kobling av MS med et HPLC instrument kunne ha redusert tiden brukt på å utvikle og bruke kvantifikasjonsmetoden betydelig.

Preface

The work and writing of this master's thesis took place at the faculty of chemistry, biotechnology and food science (KBM) at the Norwegian University of Life Sciences (NMBU) from August 2022 to November 2023. The thesis constitutes 30 ECTS as part of a 300 ECTS integrated master's degree started in 2018. The project was supervised by Professor Dag Ekeberg and senior engineer Hanne Marie Devle. That you for all your guidance and support.

Thank you to Einar Jonsson, Mehdi Mohammadi, Even Holm Hansen and Cynthia Nguyen with whom I've spent hours in the lab the last year and a half. You've been wonderful companions this past year, and spending time in the lab with you has been a joy.

During my time at NMBU, I had great help from my friend and fellow student Maria Bentzen. Thank you for countless great discussions and colloquiums, I couldn't have done it without you.

Live Solhaug

Ås, December 2023

Norwegian University of Life Sciences (NMBU)

Table of Contents

Abbreviations

3-O-C12-HSL	N-(3-oxododecanoyl)-L-homoserine lactone
3-O-C6-HSL	N-(3-oxohexanoyl)-L-homoserine lactone
AHL	N-acyl-L-homoserine lactone
C12-HSL	N-dodecanoyl-L-homoserine lactone
C14-HSL	N-tetradecanoyl-L-homoserine lactone
C4-HSL	N-butanoyl-L-homoserine lactone
C6-HSL	N-hexanoyl-L-homoserine lactone
ESI	Electrospray Ionization
MS	Mass Spectrometry
QSSM	Quorum sensing signalling molecules
LIT	Linear ion trap
RF	Radiofrequency
DC	Direct current
AC	Alternating current
m/z	Mass to charge ratio
v/v	Volume per volume
SAM	S-Adenosyl methionine
ACP	Acyl carrier protein
CID	Collision Induced Dissociation
CE	Collision energy
HPLC	High Performance Liquid Chromatography

1 Introduction

Gram negative bacteria make up a large portion of life on earth. An understanding of their methods of communication is necessary for our full understanding of their behaviours. With a deeper insight into their methods of communication we can further our understanding of when and why they perform certain behaviours, such as biofilm production, and further learn to speak their language.

Bacteria communicate through a phenomenon known as quorum sensing, which was discovered in 1970 when it was named “autoinduction”. [1] In 1994 the term was changed to quorum sensing, with the authors defining the minimal population size needed for behaviour coordination as a “quorum” of bacteria. [2] The term means, in a socio-political context, “the minimum number of people required to conduct business”. It was implemented into the context of quorum sensing bacteria as “the minimum number of bacteria required to perform certain behaviours”.

Quorum sensing involves the release of quorum sensing signal molecules (QSSMs) that - when present in adequate concentrations - can alter gene expression in the population and enable them to coordinate their behaviour according to the needs of the population.

The autoinducing molecules discovered in 1970 were identified as N-acyl homoserine lactones (AHLs) a little over a decade later and have since been studied frequently. [3] From synthetic biologists aiming to use AHLs to control bacterial communication to organic analysts aiming to identify and quantify their presence using chromatography and mass spectrometry, many people are working to further our shared scientific understanding of quorum sensing.

1.1 Problem statement

Gram negative bacteria use N-acyl homoserine lactones to facilitate intercellular communication, and knowledge of when different signal molecules are in use can help further our understanding of their language. Use of synthetic AHLs can intercept the communication and change the behaviour of bacterial populations. [4]

This project seeks to identify the presence of certain N-acyl homoserine lactones in a medium through use of direct infusion electrospray ionisation mass spectrometry. In this thesis a method for such identification is described, along with a proposed method for quantification of the same molecules.

1.2 Quorum sensing

N-acyl-L-homoserine lactones make up one set of diverse secondary metabolites that facilitate intracellular communication known as quorum sensing. When a population of bacteria "sense" a sufficient concentration of QSSMs they can have a wide range of physiological responses, all depending on the released QSSM. This mechanism allows the population to coordinate certain behaviours, such a biofilm formation or nutrient acquisition. [5] Figure 1 illustrates a simplification of the process of quorum sensing.

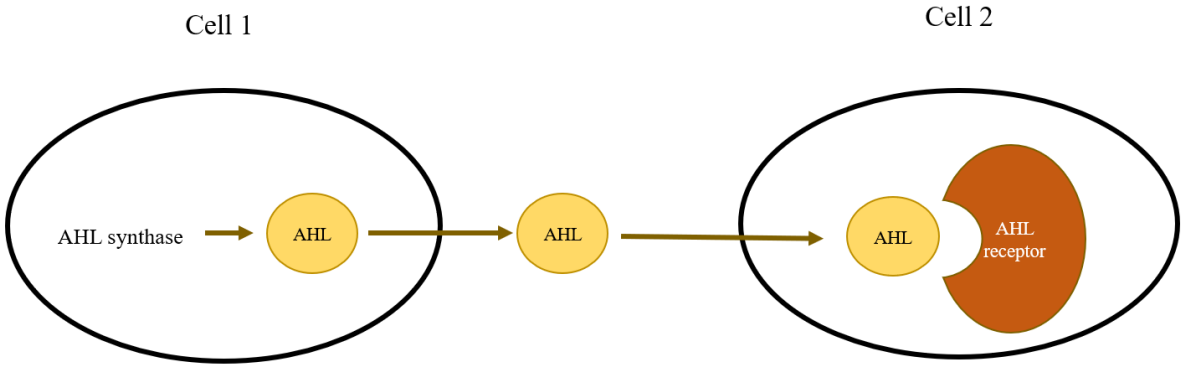

Figure 1: A simplified process of quorum sensing

The gram-negative bacteria have genes that produce AHLs synthase, which aid in the production of AHLs from SAM and Acyl ACP (see chapter 1.2.2). The AHLs are then transported out of the cell to be "sensed" by other cells. The AHL will partake in gene regulation in the cells where it's received, and behaviour will be coordinated accordingly. [6]

1.2.1 N-acyl homoserine lactones

N-acyl homoserine lactones are a group of quorum sensing signal molecules that differ in the composition of their acyl group. In this project, AHLs with the general compositions found in Figure 2 were studied. Figure 2 shows that the studied AHLs can be divided into two groups (Figure 2a and Figure 2b, that differ in their number of carbonyl groups.

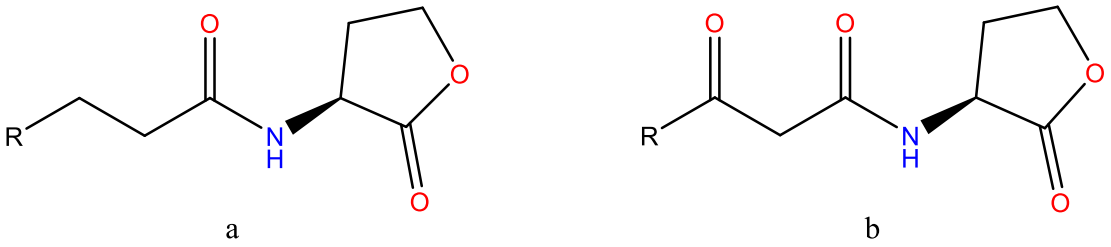

Figure 2a: Overall composition of the N-acyl homoserine lactone without oxidation, Figure 2b: Overall composition of 3-oxo-N-acyl homoserine lactone

N-butanoyl-L-homoserine lactone, N-hexanoyl-L-homoserine lactone, N-dodecanoyl-L-homoserine lactone, N-tetradecanoyl-L-homoserine lactone, N-(3-oxohexanoyl)-L-homoserine lactone and N-(3-oxododecanoyl)-L-homoserine lactone were studied in this project and are shown in Figure 3.

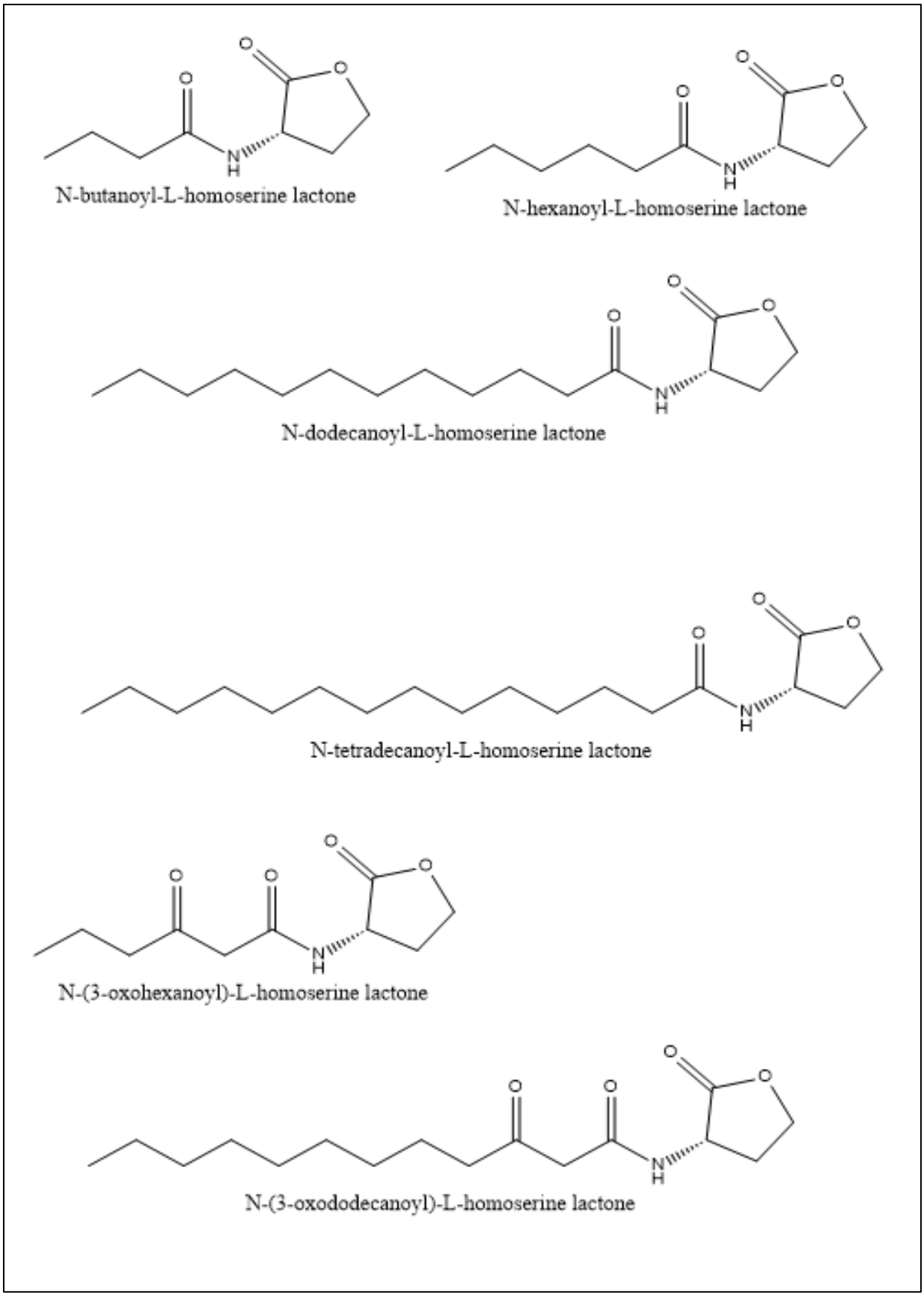

Figure 3: The structures of the six N-acyl homoserine lactones studied in this project.

1.2.2 Biosynthesis

AHLs are biosynthesized from S-Adenosyl methionine (SAM) and acyl-Acyl Carrier Protein. (acyl-ACP), Scheme I. The acyl-ACPs are biosynthesized from acetyl-CoA and malonyl-CoA through the acetate pathway prior to this interaction. [7]

SAM is biosynthesized from the amino acid methionine and adenosine triphosphate (ATP). [8]

The acetate pathway creates poly-β-keto chains from acetyl-CoA and malonyl-CoA through Claisen reactions. These reactions give rise to an additional two carbons on the chain per repeat, so the chain will always contain an even number of carbons. The chains are later reduced to give rise to acyl-ACPs which react with SAM to give the AHLs. [9]

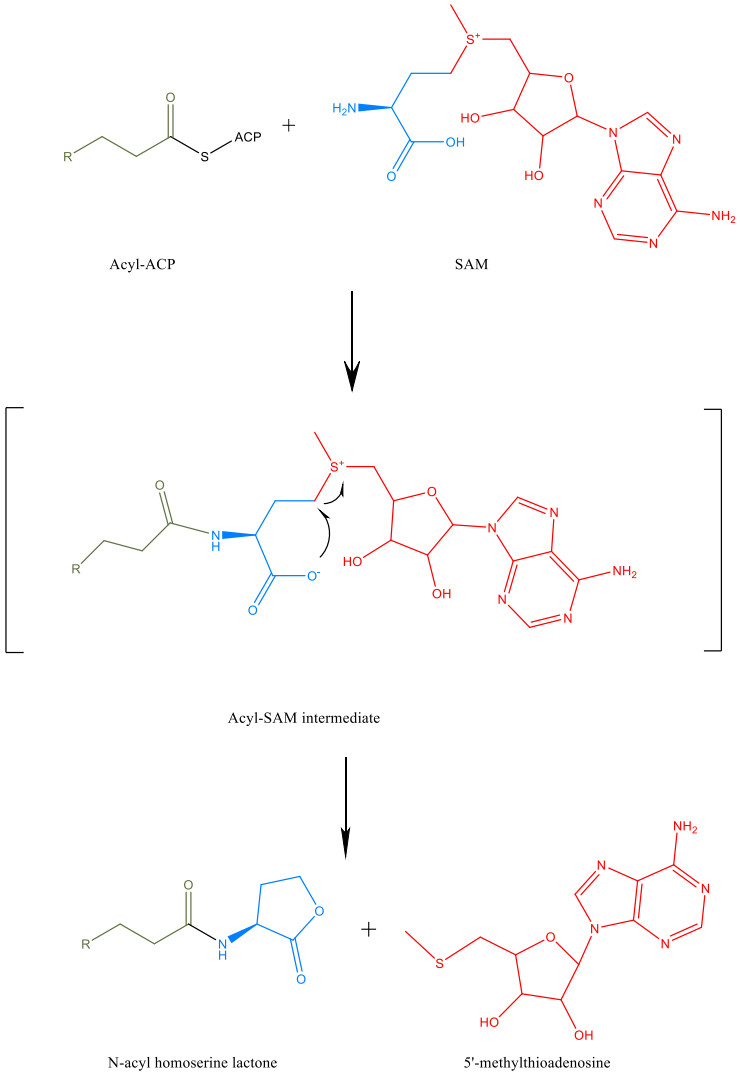

Scheme I: The biosynthesis of AHLs from acyl-ACP and SAM

In AHLs where the carbon chain contains an oxygen (carbonyl or hydroxyl group), the acyl-ACP is not fully reduced. In scheme II the biosynthesis of 3-O-C_n-HSLs is shown. In these cases, SAM reacts with a beta-keto-acyl- ACP, although the mechanisms are the same as mentioned above. [10]

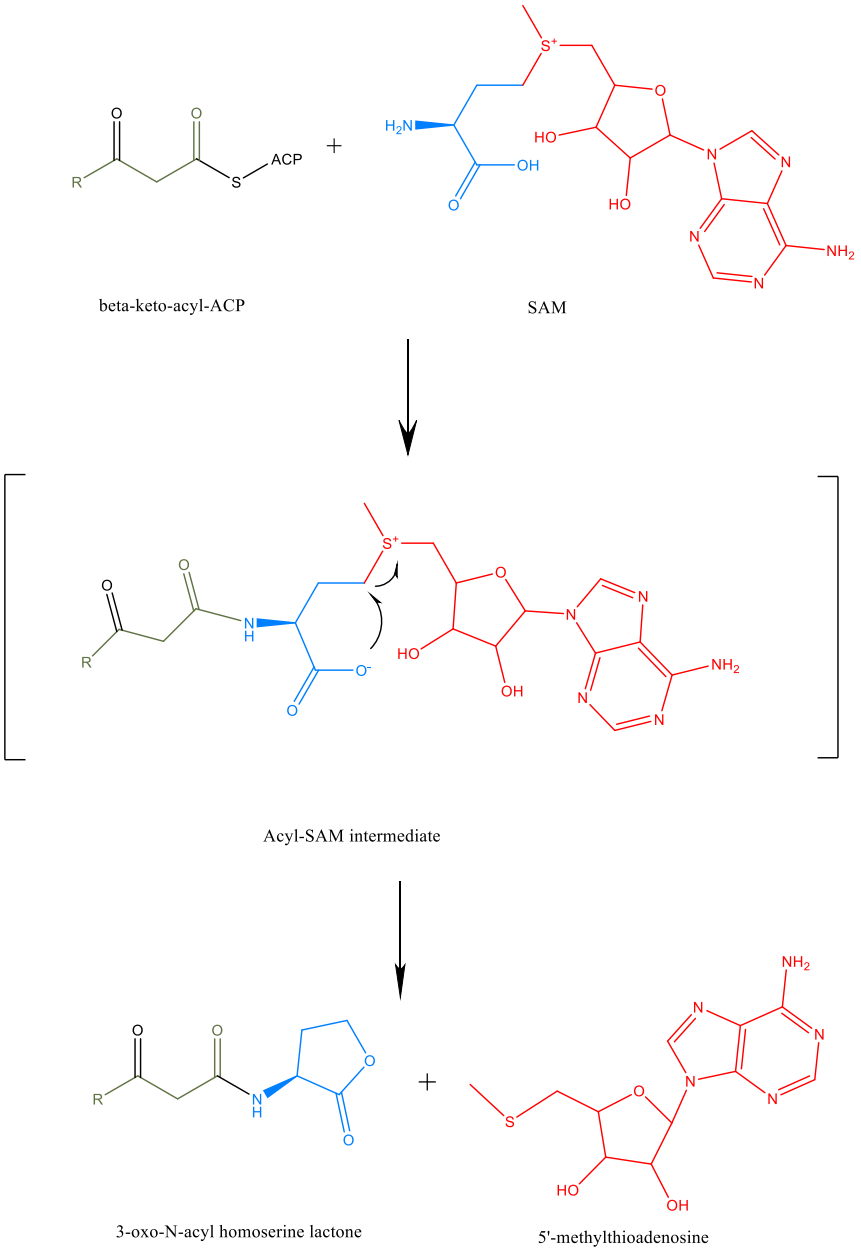

Scheme II: The biosynthesis of AHLs from beta-keto-acyl-ACP and SAM

Two AHLs that have been studied a lot are N-(3-oxododecanoyl)-L-homoserine lactone (3-O-C12-HSL) and butanoyl-L-homoserine lactone (C4-HSL), both of which are to be studied in this project.

3-O-C12-HSL and C4-HSL take part in gene regulation in two different quorum sensing systems, LasI-LasR and RhlI-RHlR respectively. The LasI and RhlI proteins catalyse the production of their respective AHLs. The AHLs then bind to their transcription factor, LasI or RhlR, which furthermore activate expression of multiple genes. In fact, the LasIR quorum sensing system activate *lasI*, *rhlI* and *rhlR*, allowing the receiving cell to continue both LasI and RhlI production, and respond to the RhlIR system with its newly synthesised RhlR transcription factor. [6]

1.2.3 Applications

Bacteria react to specific QSSMs in specific ways. By introducing the QSSMs ourselves, we can control the behaviour of the bacteria[4]. In a way, QSSMs allow us to communicate with bacteria in their language, and therefore take control of their behaviour in ways that are beneficial to us. We can also analyse their use of QSSMs to further understand why and when they use specific ones. We can essentially learn their language, listen in, and communicate back.

1.3 Mass Spectrometry

Mass spectrometry is a method of qualitative and quantitative analysis. First, the molecules are ionized, then possibly fragmented, then separated by their mass to charge ratio, and lastly detected. The detected ions are shown in a mass spectrum where the height of a peak signifies the relative abundance of the ion it represents, whether that is the precursor ion or a fragment of it. This relative abundance is calculated as a percentage of the abundance of the most abundant ion, or visually represented, the highest peak. This is called the base peak and has a relative abundance of 100 %. The abundance of every other detected ion is then compared to this base peak, and the relative abundance of said ion is defined as a percentage of the abundance of the base peak ion.

$$Relative\ abundance\ of\ x = \frac{Actual\ abundance\ of x}{Actual\ abundance\ of\ base\ peak\ ion}$$

There are several types of ionizers, analysers and detectors, and preferably one would select the combination best suited to a project's needs. There are however usually limitations in the availability of these combinations. In this experiment, electrospray ionization (ESI) was coupled with a linear ion trap mass analyser.

ESI is a soft ionisation method due to its generation of even electron ions. ESI therefore creates ions with low internal energy and will consequently create minimal fragmentation. To

create higher levels of fragmentation, addition of a collision gas to further fragment the ions is necessary[11]. First, the ESI source produces even electron ions (normally of the M-H or M+H variety, depending on whether the instrument is used in its negative or positive mode), then precursor ions chosen by the user are selected. After this, the selected ions collide with inert collision gas inside the LIT. The energy of this collision can also be controlled by the user. The collision increases the internal energy of the ions, promoting them into excited stages, which causes the ions to decompose into what is known as product ions. The product ions are then detected by a second mass analyser.

Control of collision energy, as one has when using ESI, is different from the control of the ionization energy one has when using electron ionization. Electron ionization is a hard ionization method and will create a relatively high level of fragmentation directly after ionization.

1.3.1 Electrospray Ionization

In this experiment, electrospray ionization was employed. Historically ESI was used primarily for protein analysis, but in later times its use has been extended to other polymers as well as smaller polar molecules. ESI requires the injection of a liquid and is therefore easily coupled with high-performance liquid chromatography (HPLC).

In an ESI source the sample enters an electric field through a capillary tube. This electric field arises from a high difference in potential between the capillary and a counter-electrode about 0.3 to 2 cm away, having a voltage of between 3000 and 6000 V. This results in electric field of order 10^6 V/m. To achieve a stronger electric field with a lower voltage, the distance between the capillary and the counter-electrode would need to be reduced. A charge accumulation in the liquid at the surface of the capillary will be induced by the electric field forming a Taylor cone, and highly charged droplets will emerge from the capillary. [12]

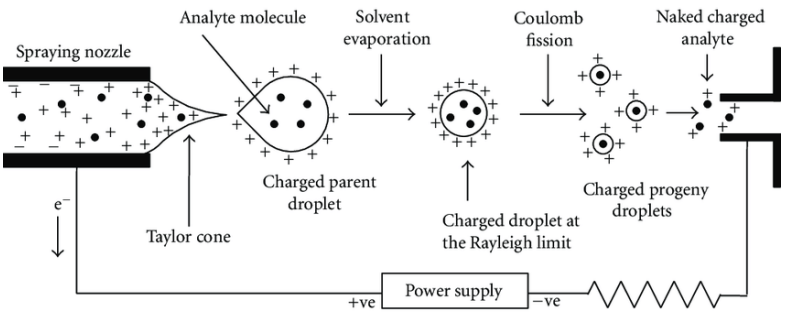

Figure 4: Schematic representation of electrospray ionization. Redistributed from Banerjee and Mazumdar. [13]

1.3.2 Analyser and Detector

Ions exit the ESI and enter the mass analyser. In this experiment, a linear ion trap was used. The LIT separates the ions based on their resonance frequency and is based on another analyser known as the quadrupole. [12]

A quadrupole analyser consists of four perfectly parallel rods of oscillating potential. A positive ion will be drawn to a negative rod, whose potential will shift and become positive. Unless the ion has already reached the rod, it will shift trajectory. If the ion is light, its trajectory is easily altered, allowing it to readily move away from the positive rod and towards the newly negative rod. On the contrary, the trajectory of a heavy ion will not as easily adapt to the oscillations. The goal is to only allow ions of a certain *m/z* to pass through the quadrupole in its entirety. Ions that have an *m/z* lower than optimal will move too quickly and discharge onto the rod with the opposite charge before it reaches the end, whereas the trajectories of ions with a higher than optimal *m/z* will not shift rapidly enough and will discharge onto the rod with the same charge as itself. The exact *m/z* ratio allowed though the quadrupole can be set to change over time, allowing scans to take place. [12]. Scans search through all the *m/z* ratios within a defined interval over a short amount of time. All ions with a *m/z* within that interval will be detected, at rates that depend on their abundance.

The potential applied to the quadrupole rods can be expressed through the equation $\Phi_0 = U - Vcos\omega t$ where ω is the angular frequency expressed in radians per second, U is the DC applied to the rod and V is the amplitude of the RF voltage. The positive rods have the potential, Φ_0 and the negative rods have the potential $-\Phi_0$. The absolute value of the potentials will be equal, so they can be described as Φ_0 and -Φ_0, where Φ_0 has a distinct value at a certain point in time. The angular velocity is constant at $\omega = 2\pi\nu$ ($being$ the RF frequency), a change in the potentials must arise from a change in the remaining variables, U and V. Changing the potentials is done to switch from one *m/z* to another.

With the instruments being three-dimensional, defining axes as x, y and z be useful. A common definition is that the z-axis is parallel with the rods of the quadrupole, while x and y arise perpendicular to both the z-axis and each other. The x and y axes each go through rods of equal potential.

An ion will maintain constant velocity along the z-axis, yet the forces from the electric field that arises in the quadrupole will accelerate said ion in both x and y directions. This gives the ion trajectories a spiral shape.

The LIT, being based on the quadrupole, builds further on these principles. It has a quadrupolar field that confines the ions in the radial dimension (the x and y axes described above) and lenses on the front and back section that create an electric field in the axial dimension (the z-axis describes above). The ions can in theory escape the analyser through axial or radial ejection, axial ejection being the route known from the quadrupole for the optimal *m/z* and radial ejection being through the slots between the rods. Radial ejection is however not found in commercial instruments.

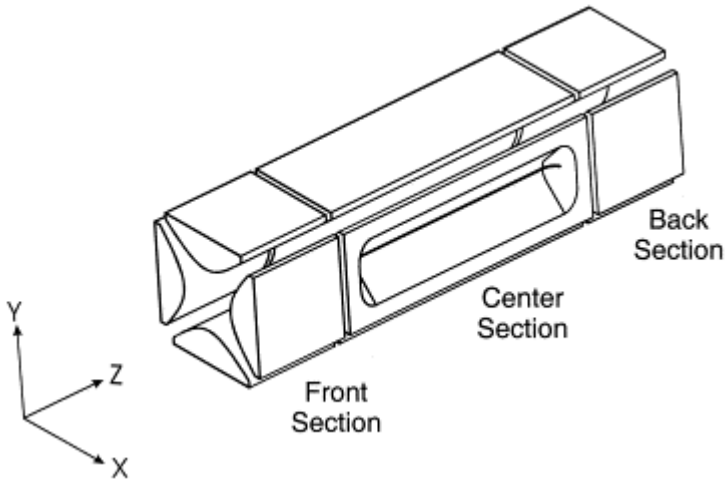

Figure 5: Basic design of a 2D linear ion trap. Redistributed from Schwartz et. al. [14]

LIT with axial ejection was invented in 2001. [15] AC voltages between the rods and the exit lenses create a field that expels the ions. This field only expels the ions closed to the exit lens, so the ejection efficiency is considered quite low. This efficiency can be improved by the addition of lenses between each rod, generating an electrostatic potential and that is steady along what is here defined as the z-axis.

1.3.3 Fragmentation

As the compounds get positively ionized in the ESI, several of them will split into smaller fragments. The prevalence of a fragmentation reaction depends on how much collision energy is provided in the ESI, where a higher energy results in more fragmentation. These fragments will show up as peaks in the final mass spectrum, alongside the potential precursor ions if those are still present. There are several different types of fragmentation, some more common than others. This chapter will give an overarching idea of these types and this theory will be applied to the AHLs of interest in a later chapter.

The heterolytic bond cleavage splits the molecule into a positive and a negative ion. However, seeing as the precursor structure is an ion, the resulting fragments become a positive ion and a neutral fragment.

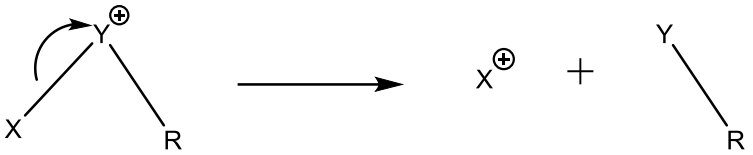

Scheme III: The mechanism of heterolytic bond cleavage

The positive ion that follows from such a reaction, above labelled X, needs to be relatively stable. The stability of X, as well as the collision energy, will determine the abundance of *m/z* M_X, where M_X is the mass of the fragment X. In the reaction above the charge migrated from Y to X, which makes it a charge migration fragmentation (CMF). CMF is a group of fragmentations that move the charge site to a new location and cause a behind a neutral fragment.

Fragmentations without migration of the charge site are called charge retention fragmentations (CRF) and include Retro-Diels-Alder (RDA), remote hydrogen rearrangements, aromatic eliminations, radical fragmentation and McLafferty rearrangement where the fragmentation commonly occurs at a remote location from the charge site.

The homolytic bond cleavage splits the molecule into two radicals, each side gaining one electron from the split of the bond. In positive ESI, original compound was a positive ion, and the fragmentation will therefore generate either X^{*+} or Y^{*+}, which are called distonic ions. [11] These can occur anywhere in the structure, and do not cause charge migration.

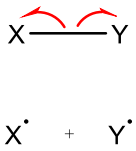

Scheme IV: The mechanism of homolytic bond cleavage

With knowledge of the structure of the precursor ion, figuring out which fragmentation reactions are possible is an ideal starting point to figuring out which ones can describe the different peaks in the spectrum. Demarque et. Al. describe nine different CRF fragmentations acquired from positive ESI MS analysis. An aromatic elimination, for example, is not possible with an AHL starting point, as it requires a chain with at least four conjugated double bonds (Scheme 5)

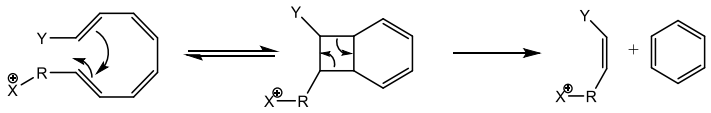

Scheme V: The mechanism of aromatic elimination

One form of fragmentation that is known to occur is remote hydrogen rearrangements, depicted in scheme VI. This is a fragmentation reaction that is relatively common.

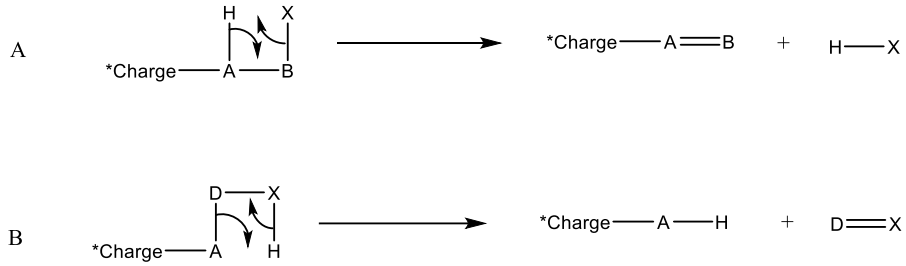

Scheme VI: The mechanism of remote hydrogen rearrangement

A fragmentation reaction of this nature involves an intramolecular 1,2-elimination, creating a π bond in either the detected fragment ion (option A) or in the eliminated neutral molecule (option B).

Another CRF reaction that can occur is a carbon monoxide elimination from a cyclic carbonyl compound (Scheme VII). Lactones are cyclic carbonyl compounds and are therefore eligible for this kind of reaction.

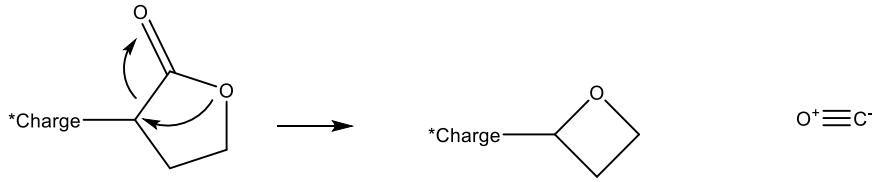

Scheme VII: The mechanism of carbon monoxide elimination from a cyclic carbonyl compound

In scheme VII the structure of the lactone group in AHLs is shown, as opposed to scheme IV which illustrates a general mechanism. The ring does not need to be of this size, nor does it need to be a lactone. The mechanism is possible for any cyclic carbonyl compound.

1.4 Theory behind the method of identification

To identify the presence of each individual AHL, one would have to know how they fragment. By learning what fragments explain the presence of a specific molecule, they can be found and identified in a mass spectrum.

When searching for AHLs using the protonated molecular ion, a peak often forms at *m/z* 102. [16] This ion defines a neutral loss of the acyl chain, leaving behind the same lactone ring in fragmentation of all the AHLs. This is the ion that will be detected. C_nH_{2n+1} is a common fragmentation, resulting in loss of *m/z* 15, 29, 43, 57, and so on. The ions fragment in the ESI to create a particular pattern for a particular structure.

Using this knowledge, one would have to either search through a library of spectra or interpret the spectra manually. In this project, this part of the identification process must be done manually. To work out what a particular structure fragments to, one would need to use standards in a solution without interfering ions.

A spectrum will show lines for the detected ions, ranging in size based on relative abundance. The largest *m/z* of interest represents the mass of the precursor ion, if present. From there one would calculate the loss of mass for another line. If the precursor ion has a mass of 172 and there's a peak at *m/z* 144 this corresponds to loss of 28 amu, representing CO or C_2H_4.

When one is familiar with the structure, figuring out the fragmentation is often a simpler task than if handed a spectrum with no idea what it represents. When attempting to recognize the fragments of a known structure, a method of trial and error is not unheard of.

When employing ESI, *m/z* = M (where M is the mass of a pseudomolecular ion of a particular AHL) will be selected and its fragments analysed. If *m/z* = M is present, the fragmentation needs to be studied closer to figure out if the precursor ion was the AHL in question, or another structure with the same mass.

1.5 Theory behind the proposed method of quantification

The method outlined in this thesis uses external standard curves to determine the concentrations of certain chemicals in solvent. Instead of creating the more traditional standard curve - a two-dimensional regression model of that seeks to find the linear relationship between X and Y – a multiple linear regression model with two explanatory variables was chosen, seeking to find a relationship between X_1, X_2 and Y. If the equation were to be graphed, it would be three dimensional.

$$Y = \beta_0 + \beta_1 X_1 + \beta_2 X_2$$

The software used grants output of both relative and actual abundance of ions. The actual abundances of pseudo molecular ions can be used to create these standard curves, one for each analyte. Applying a low collision energy would allow for low fragmentation, which is a useful approach when the only pseudo molecular ions are of interest. Applying this theory to the abundance of $[M+H]^+$ and $[M+Na]^+$ ions, one could determine the concentration with hopefully greater accuracy than when using a normal standard curve with only one explanatory variable. Inserting the abundance as the explanatory variable X, the concentration can then be defined as Y.

Seeing as hydrogen has a mass of 1 amu, and sodium has a mass of 23 amu, the abundance of the ions can be described as A_{M+1} and A_{M+23} respectively. The equation can therefore be described as follows:

$$C = \beta_0 + \beta_1 A_{M+1} + \beta_2 A_{M+23}$$

Theoretically, an attempt to expand to more pseudo molecular ions could be considered possible, if it were not for the caution advised when adding more variables to a statistical model. If the goal can be achieved with two explanatory variables, one should not add more.

2 Experimental

2.1 Materials and equipment

2.1.1 Chemicals

The following chemicals were utilized in this project.

Table 1: A list of utilized chemicals, along with quality and supplier.

Chemical	Quality	Supplier
Methanol	HiPerSolv Chromanorm ®, ≥ 99.9 %	VWR Avantor
Acetonitrile	HPLC gradient grade, ≥ 99.9 %	Sigma-Aldrich
Formic Acid	ACS reagent, ≥ 96%	Sigma-Aldrich
N-butanoyl-L-homoserine lactone 5 mg	≥ 95 %	Cayman Chemical
N-hexanoyl-L-homoserine lactone 5 mg	≥ 95 %	Cayman Chemical
N-dodecanoyl-L-homoserine lactone 5 mg	≥ 98%	Cayman Chemical
N-tetradecanoyl-L-homoserine lactone 5 mg	≥ 98 %	Cayman Chemical
N-(3-oxo-hexanoyl)-L-homoserine lactone 5 mg	≥ 95 %	Cayman Chemical
N-(3-oxo-dodecanoyl)-L-homoserine lactone 5 mg	≥ 98 %	Cayman Chemical

The solvent consisted of 1% formic acid, 4% acetonitrile and 95% methanol. This solvent was used to create solutions and to dilute already prepped solutions, as to easily maintain the composition of the solvent for solutions where the analytes occurred in separate concentrations. A 500 mL flask of solvent was prepared and used throughout the entire experiment, though refilling it was necessary.

Acetonitrile is a common solvent for MS analysis of QSSMs, while using a mixture of formic acid and acetonitrile has been shown to be useful as a mobile phase in HPLC-MS for analysis of the same compounds. [17] In this project, HPLC was not employed, but seeing as the analytes elute solved in said mobile phase, knowledge of its constitution is relevant and the chemical was therefore used in this project.

2.1.2 Analytes

The following chemicals, all AHLs, were the analytes in this research. Their masses and relevant theoretical MS peaks are listed as well (Table 2).

Table 2: Mass and pseudomolecular ions for each analyte studied in this project.

Analyte	Mass (amu)	Theoretical [$M+H^+$]	Theoretical [$M+Na^+$]
C4-HSL	171.2	172.2	194.2
C6-HSL	199.2	200.2	222.2
C12-HSL	283.4	284.4	306.4
C14-HSL	311.5	312.5	334.5
3-O-C6-HSL	213.2	214.2	236.2
3-O-C12-HSL	297.4	298.4	320.4

2.1.3 Instruments and software

The analysis utilized an ESI-linear ion trap mass spectrometer (LTQ XL, Thermo Fisher Scientific, Waltham, MA, USA) for fragmentation and detection. Operating in positive mode, the electrospray voltage was set to 4.5 kV. The transfer capillary maintained a temperature of 275 °C, with a sweep and auxiliary gas flow of 5.00 arb. units, and a sheath gas flow of 40.00 arb. units. Xcalibur 2.2 SP1.48 (Thermo Fisher Scientific, Waltham, MA, USA) facilitated method setup and data acquisition, while instrument control was controlled by Thermo Tune Plus. Detailed configurations of the programs created in Xcalibur can be found in subsequent chapters, seeing as the qualitative method and the quantitative method needed different setups.

The solution that was to be analysed was introduced to the transported to the instrument via direct infusion by a Hamilton syringe, although the mass spectrometer was linked to a Thermo Scientific Dionex UltiMate 3000 UHPLC through the Xcalibur software. An empty LC vial was therefore placed in the autosampler of the LC instrument to make the system run smoothly.

For the proposed idea for a quantitative method, RStudio was used to identify the relationship between the concentration and the abundance of ions detected, as described in chapter 1.5.

2.2 Qualitative method

The analytes that were used belong to one group of QSSMs, the N-acyl-L-homoserine lactones. Distinctions within the group arise from the differences in length and/or substitutions of the acyl chain present.

2.2.1 Identification of the optimal collision energy

Preparation

Analysis without coupling with HPLC was of interest, and so it was completed with direct infusion with a Hamilton syringe as to allow all analytes to enter the MS simultaneously. The ion source was an electrospray ionizer coupled with a linear ion trap for mass analysis.

The method development process started by identifying the optimal collision energy for identification. Ideally keeping the pseudo molecular peak at 10-20 % of the base peak. Analytes were solved in the solvent at a concentration of 0.1 mg/mL.

Getting the analytes out of their vials in known amounts turned out to be a difficult task, and therefore a method of dropping open vials into blue cork flasks and adjusting the volume of solvent was selected. 5 mg of analyte was in this way solved in 50 mL solvent, yielding a concentration of 0.1 mg/mL.

Software settings

The ESI was set to positive ion searching using the Xcalibur and Tune Plus softwares. When creating the programs in Xcalibur, CID was performed at different collision energies, ranging from 5 – 100 eV with increments of 5 eV.

Use of CID was the best option, seeing as there was a need for identifying the presence of different components in a solution. CID would allow further fragmentation of ions with a selected m/z ratio.

An optimal collision energy had to be identified and therefore CID was done at multiple collision energies. The optimal collision energies were then determined for each individual AHL from the spectra by finding spectra where the pseudomolecular ion peaks were between 10 and 20 % of the base peaks, or as close to this ideal as possible. From there, identifying peaks were found and the structures of the fragments determined. See Table A.I. for the general setup of this program. Two of these programs were run for each AHL, one for $M+H^+$ and one for $M+Na^+$. Between each run, the instrument was cleaned with methanol until no peaks from the previous AHL showed up in the spectrum.

2.2.2 Identifying the presence of individual AHLs

By employing the already identified optimal collision energy and knowledge of identifying peaks, one can create a program that searches for each individual pseudomolecular ion at its optimal CI and finds its fragments. A new solution containing all the analytes was prepared and a new program was made using the identified optimal collision energies, they were adjusted to fit the ideals better, and the same solution was run 5 times to check instrumental reproducibility.

With knowledge of diagnostic peaks identified using the last program, one can deduce if a value of M represents the AHL of interest or if it is another structure with a similar mass. The CI values and fragments are considered results in this thesis and will be provided in chapter 3.

2.3 Proposed idea for method of quantification

2.3.1 Identification of the optimal collision energy

The optimal collision energy for quantification is going to be different than the energy used for qualitative analysis. The ideal spectra have base peaks that represent pseudomolecular ions, as opposed to the ones described in chapter 2.2.1.

The *m/z* ratios of interest are the protonated molecular ions and sodium adducts, and their masses are listed in table 1.

Selected ion monitoring was completed at multiple collision energies, namely 20, 40, 60, 80 and 100 eV. The optimal collision energy was then determined from the spectra by finding spectra where the pseudomolecular ion peaks are the base peaks. None of which was deemed useful, and 10 eV was used.

2.3.2 Preparing a standard curve

The spectra show the genuine abundance of the ions as opposed to relative abundance; therefore, the height of peaks can be directly linked to the concentrations of the analytes. Seeing as there are two masses of interest per analyte ($[M+H]^+$ and $[M+Na]^+$) the concentration of an analyte relates to two separate numbers, namely the abundances of these masses in a spectrum. Using multiple linear regression to calculate the concentration in a sample is a sensible approach. The relationship between the abundances and the concentration should be linear, so the standard curve will be following the equation below.

$$y = \beta_0 + \beta_1 x_1 + b_2 x_2$$

In this model, the variable y represents the concentration of the analyte in question, x_1 represents the abundance of $[M+H]^+$ at the optimal collision energy, x_2 represents the abundance of $[M+Na]^+$ at the optimal collision energy, wherein M describes the analyte in question. In this case, the relationship can be described as $C = \beta_0 + \beta_1 A_{m+1} + \beta_2 A_{m+23}$, where C is the concentration of the analyte, A_{m+1} is the abundance of $[M+H]^+$ ions and A_{m+23} is the abundance of $[M+Na]^+$

The parameters β_0, β_1 and β_2 are to be determined from analysing several known concentrations of the analytes and finding their respective abundances. The parameter β_0 should be equal to 0, and can be forced to be, as it represents the concentration when there is no peak representing the molecular ion. This approach requires one regression curve to be constructed per analyte and employing them all separately when analysing samples. Several parallels at each concentration should be analysed, to account for variation that might arise in preparation of the samples as well as in the instrumental analysis.

These formulas will be created in RStudio, and statistical significance will be checked. RStudio will show an R^2 value, which describes what amount of variance in Y can be attributed to the variance in the Xs, in other words how fit the model is for quantification. T-values and p-values will also be found, describing the certainty of a relationship between the values of Y and the values of the Xs.

3 Results and discussion

The main objective of the project was to construct a method for identification of C4-HSL, C6-HSL, C12-HSL, C14-HSL, 3-O-C6-HSL and 3-O-C12-HSL using direct infusion ESI-MS. The resulting spectra need to be interpreted manually.

3.1 Results from identification method

The spectra discussed in this chapter can be found in A.I – A.XII. The spectra shown in the appendix were rendered using Collision-Induced Dissociation (CID). The method of preparation listed in chapter 2, and the resulting optimal CE are listed in Table 3 showing the final program.

Alongside finding the optimal CE, the fragments were also identified.

Table 3: Optimal collision energies discovered for MH^+ and MNa^+ for all six analytes.

Time start (min)	Time stop (min)	*m/z*	CE (eV)	Analyte
0	0.3	172.2	25	C4-HSL + H^+
0.4	0.7	200.2	30	C6-HSL + H^+
0.8	1.1	284.4	25	C12-HSL + H^+
1.2	1.5	312.5	25	C14-HSL + H^+
1.6	1.9	214.2	25	3-O-C6-HSL + H^+
2.0	2.3	298.4	25	3-O-C12-HSL + H
2.4	2.7	194.2	25/30	C4-HSL + Na
2.8	3.1	222.2	25/30	C6-HSL + Na
3.2	3.5	306.4	30	C12-HSL + Na
3.6	3.9	334.5	25/30	C14-HSL + Na
4.0	4.3	236.2	25/30	3-O-C6-HSL + Na
4.4	4.7	320.4	25/30	3-O-C12-HSL + Na

After repeating the analysis for the protonated molecules (of which C6-HSL required 30 eV), CID on *m/z* 200.2 yielded a peak of << 10 % of the base peak, and 25 eV was employed for all analytes. Which CE was optimal in the first place is up for interpretation, as the relative abundances never match the ideal perfectly.

3.1.1 Fragments of N-butanoyl-L-homoserine lactone

The spectrum of N-butanoyl-L-homoserine lactone can be found in Figure B.I. and Figure B.II. under Appendix B. The presence of N-butanoyl-L-homoserine lactone (C4-HSL) can be determined by finding the peaks *m/z* 172, 144 and 102 in a $M+H^+$ mass spectrum, which correspond to the fragments found in Figures 6, 7 and 8. In addition by finding the peaks *m/z* 194, 166 and 150 in a M+Na mass spectrum., which correspond to the fragments found in Figures 9, 10 and 11. The presence of these peaks, as well as the abundance of the ions being similar, describes exactly how the molecules fragment. Seeing as the instrument was set to CID of *m/z* 172 and later *m/z* 194, any peaks that show up in such the spectra will have precursor ions of those masses. If the mass of the precursor ion and the mass of the product ions all match up with the structure of interest one can conclude with the presence of the substance.

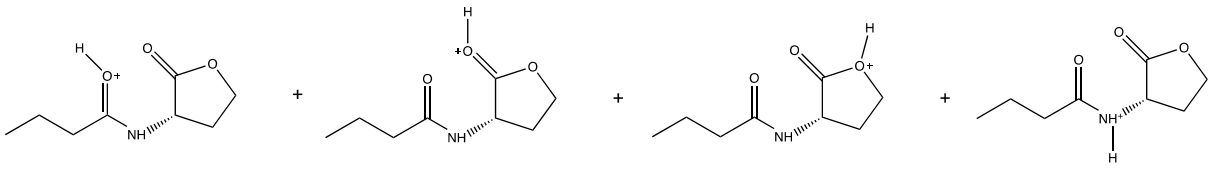

Figure 6: Structures of protonated C4-HSL (m/z 172) with different possible placements for the charge.

Figure 6 illustrates a protonated N-butanoyl-L-homoserine lactone structure. The spectra shown in appendix B show that this structure is relatively stable under a collision energy of 25 eV, although not stable enough to be the base peak.

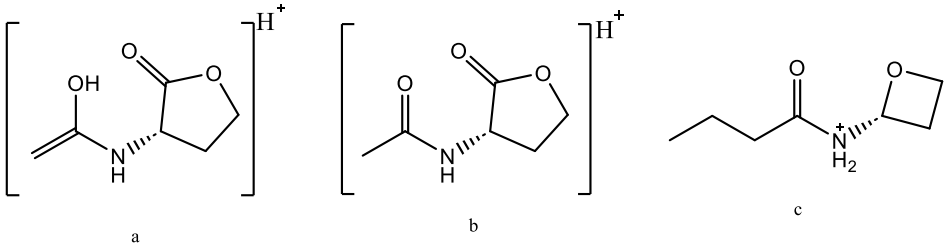

Figure 7: Proposed structures of the fragment with m/z 144 derived from protonated C4-HSL through remote hydrogen rearrangement (a, b) and carbon monoxide elimination (c).

Figure 7 illustrates a possible fragment from the protonated C4-HSL structure. The proposed fragmentation a remote hydrogen rearrangement 1.3.3 (a, b) and a carbon monoxide elimination, which is also described in chapter 1.3.3 (c). The placement of the charge in Figure 4 a and b would ideally be a remote as possible to create a minimal amount of tension, and therefore be placed on the oxygen atom furthest to the right.

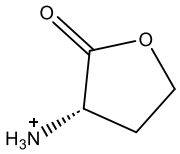

Figure 8: Proposed structure of the fragment with m/z 102 derived from C4-HSL.

Figure 8 illustrates the structure of the fragment with *m/z* 102 that is known to appear in spectra from AHLs. In the CID spectrum of N-butanoyl-L-homoserine lactone ($M+H^+$), this ion forms the base peak.

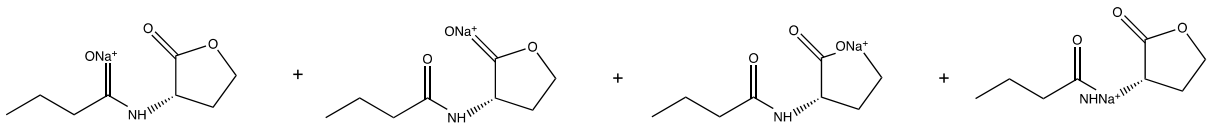

Figure 9: Structures of C4-HSL sodium pseudomolecular ions (m/z 194)

Figure 9 illustrates the structure of N-butanoyl-L-homoserine lactone ionized with sodium. This structure is the same as the one shown in Figure 6, but ionized with sodium instead of with hydrogen. This will be the precursor ion when performing CID on *m/z* 194, as is done when searching for the sodium ions instead of the protonated molecules.

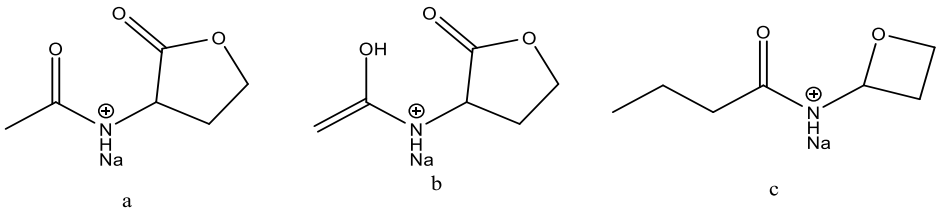

Figure 10: Proposed structures of the fragment with m/z 166 derived from C4-HSLNa⁺ through remote hydrogen rearrangement (a, b) and carbon monoxide elimination (c)

Figure 10 illustrates a structure derived from N-butanoyl-L-homoserine lactone through a remote hydrogen rearrangement (a, b). Another possibility is a carbon monoxide elimination from cyclic carbonyl compounds (c).

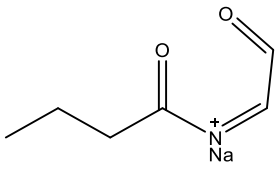

Figure 11: Proposed structure of the fragment with m/z 150 derived from C4-HSL.

Figure 11 also illustrates a structure derived from N-butanoyl-L-homoserine lactone through a remote hydrogen rearrangement.

3.1.2 Fragments of N-hexanoyl-L-homoserine lactone

The spectrum of N-hexanoyl-L-homoserine lactone can be found in Figure B.III. and Figure B.IV. under Appendix B. The presence of N-hexanoyl-L-homoserine lactone (C6-HSL) can be determined by finding the peaks *m/z* 200, 172, 158 and 102 in a $M+H^+$ mass spectrum, which correspond to the fragments found in Figures 12, 13, 14 and 15. In addition by finding the peaks *m/z* 222, 194 and 178 in a M+Na mass spectrum., which correspond to the fragments found in Figures 16, 17 and 18. The presence of these peaks, as well as the abundance of the ions being similar, describes exactly how the molecules fragment. Seeing as the instrument was set to CID of *m/z* 200 and later *m/z* 222, any peaks that show up in such the spectra will have precursor ions of those masses. If the mass of the precursor ion and the mass of the product ions all match up with the structure of interest one can conclude with the presence of the substance.

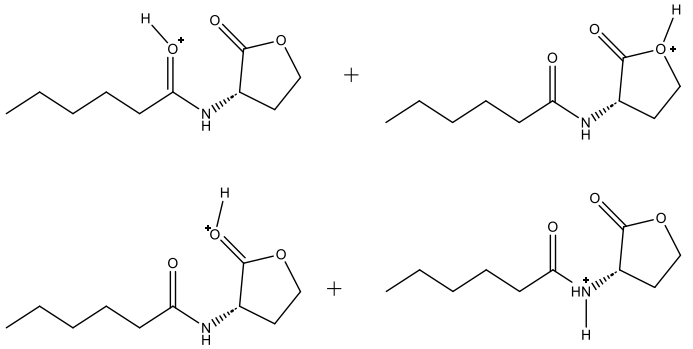

Figure 12: Structures of protonated C6-HSL (m/z 200) with different possible placements for the charge.

Figure 12 illustrates a protonated N-hexanoyl-L-homoserine lactone structure, with an *m/z* ratio of 200. This is the precursor ion when performing CID on *m/z* 200.

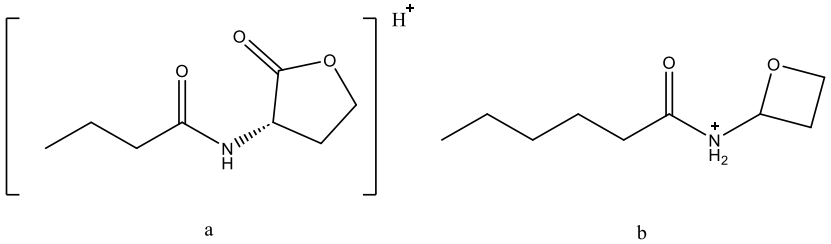

Figure 12: Proposed structures of m/z 172 fragment from protonated C6-HSL by remote hydrogen rearrangement (a), or by carbon monoxide elimination (b).

Figure 13 illustrates another fragmentation that can be explained by either remote hydrogen rearrangement (a) or carbon monoxide elimination (b), following the same fragmentation

reactions shown in figure 7. The fragment has a *m/z* ratio of 172. The structures are like the structures found in figure 7, with a longer acyl group, due to the different precursor ion.

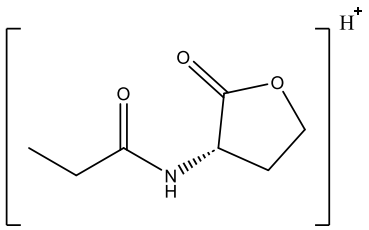

Figure 14: Proposed structure of m/z 158 fragment from protonated C6-HSL by remote hydrogen rearrangement

Figure 14 illustrates a fragment from a remote hydrogen rearrangement of N-hexanoyl-L-homoserine lactone, the same reaction seen in several other fragments. This fragment has an m/z ratio of 158.

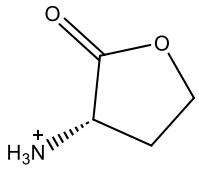

Figure 15: Proposed structures of m/z 102 fragment from protonated C6-HSL by remote hydrogen rearrangement

Figure 15 illustrates another fragment from a remote hydrogen fragmentation of N-hexanoyl-L-homoserine lactone, the previously mentioned *m/z* 102 fragment which is commonly found in ESI spectra of AHLs.

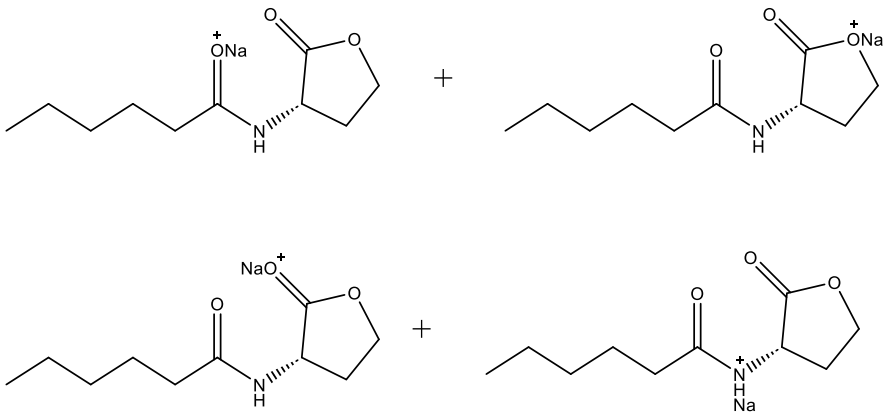

Figure 16: Structures of C6-HSL sodium pseudomolecular ions (m/z 222) with different possible placements for the charge

Figure 16 illustrates the structure of N-hexanoyl-L-homoserine lactone ionized with sodium. This structure is the same as the one shown in figure 9 but ionized with sodium instead of

protonated. This will be the precursor ion when performing CID on *m/z* 222, as is done when searching for the sodium ions instead of the protonated molecules mentioned above.

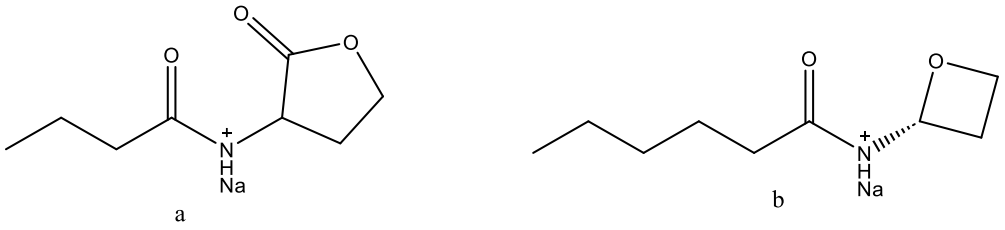

Figure 17: Proposed structures of m/z 194 fragments from C6-HSLNa⁺ by remote hydrogen rearrangement (a), or by carbon monoxide elimination (b).

Figure 17 illustrates potential fragments of the pseudomolecular structure (Figure 13) with *m/z* 194. The fragments arise from a remote hydrogen rearrangement (a), and carbon monoxide elimination (b).

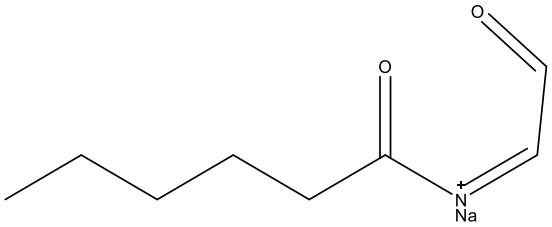

Figure 18: Proposed structure of m/z 174 fragments from C6-HSLNa+.

Figure 18 illustrates a fragment of C6-HSLNa$^+$, with an m/z ratio of 174.

3.1.3 Fragments of N-dodecanoyl-L-homoserine lactone

The spectrum of N-dodecanoyl-L-homoserine lactone can be found in Figure B.V. and Figure B.VI. under Appendix B. The presence of N-hexanoyl-L-homoserine lactone (C12-HSL) can be determined by finding the peaks *m/z* 284, 268, 256, 238, 228, 186 and 102 in a $M+H^+$ mass spectrum, which correspond to the fragments found in Figures 19-25. In addition by finding the peaks *m/z* 306, 290, 278, 276, 236 and 124 in a $M+Na^+$ mass spectrum, which correspond to the fragments found in Figures 26-31. The presence of these peaks, as well as the abundance of the ions being similar, describes exactly how the molecules fragment. Seeing as the instrument was set to CID of *m/z* 284 and later *m/z* 306, any peaks that show up in such the spectra will have precursor ions of those masses. If the mass of the precursor ion and the mass of the product ions all match up with the structure of interest one can conclude with the presence of the substance.

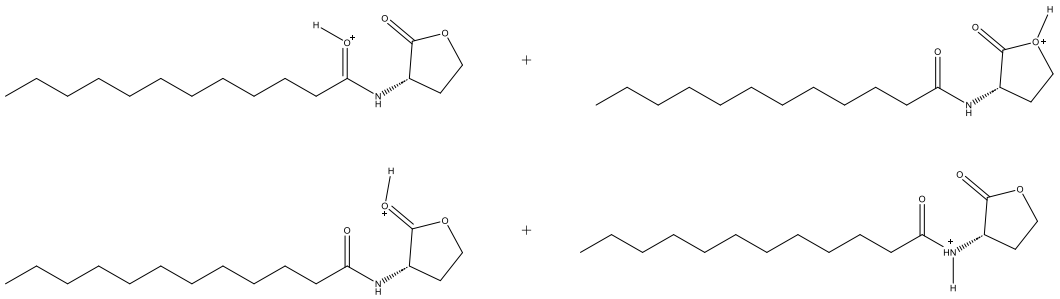

Figure 19: Structures of protonated C12-HSL (m/z 284) with different possible placements for the charge.

Figure 19 illustrates a protonated N-dodecanoyl-L-homoserine lactone ion with an *m/z* ratio of 284. This is the precursor ion when performing CID on *m/z* 284.

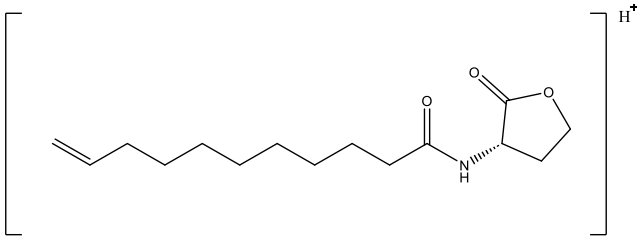

Figure 20: Proposed structures of m/z 268 fragment from protonated C12-HSL by a remote hydrogen rearrangement

Figure 20 illustrates a fragment (*m/z* 268) of the structure shown in Figure 19 (protonated C12-HSL). The fragmentation reaction which formed this structure was a remote hydrogen rearrangement, where the double bond created ended up on the detected ion as opposed to the neutral molecule.

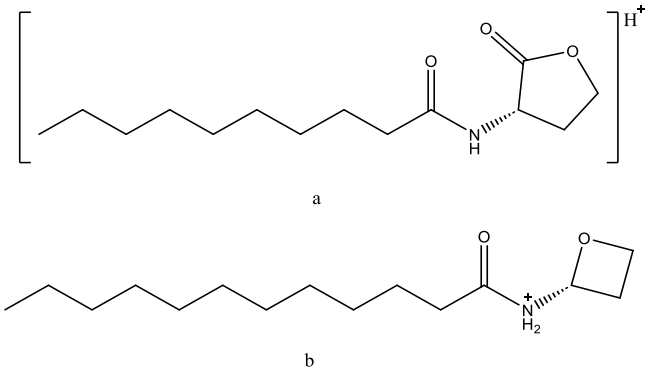

Figure 21: Proposed structures of m/z 256 fragment from protonated C12-HSL by remote hydrogen rearrangement (a), or by carbon monoxide elimination (b).

Figure 21 illustrates fragments (m/z 256) of protonated C12-HSL. These fragments arise from remote hydrogen rearrangement (a) and carbon monoxide elimination (b).

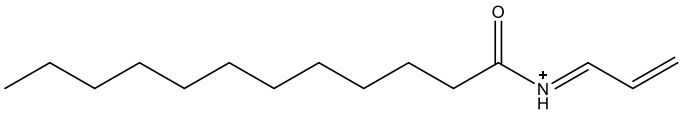

Figure 22: Proposed structure of a fragment (m/z 238) of protonated C12-HSL.

Figure 22 illustrates a fragment (m/z 238) of protonated C12-HSL.

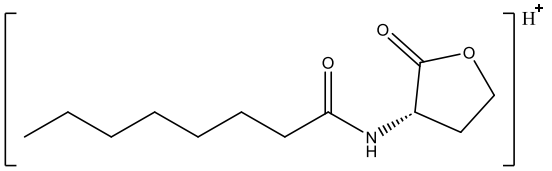

Figure 23: Proposed structure of m/z 228 fragment of protonated C12-HSL by a remote hydrogen rearrangement

Figure 23 illustrates a fragment (m/z 228) of C12-HSLNa$^+$. The fragmentation reaction which formed this structure was a remote hydrogen rearrangement, where the double bond created ended up on the neutral molecule as opposed to on the detected ion.

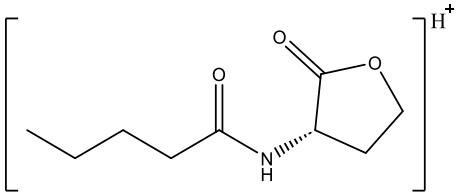

Figure 24: Proposed structures of m/z 186 fragment of protonated C12-HSL by a remote hydrogen rearrangement

Figure 24 illustrates a fragment (m/z 186) of the structure seen in figure 17. The fragmentation reaction which formed this structure was a remote hydrogen rearrangement,

where the double bond created ended up on the neutral molecule as opposed to on the detected ion.

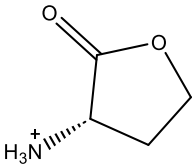

Figure 25: Proposed structures of m/z 102 fragment from protonated C12-HSL by remote hydrogen rearrangement

Figure 25 illustrates the previously mentioned *m/z* 102 fragment, this time fragmented from protonated N-dodecanoyl-L-homoserine lactone by remote hydrogen rearrangement, where the double bond created ended up on the neutral molecule as opposed to on the detected ion.

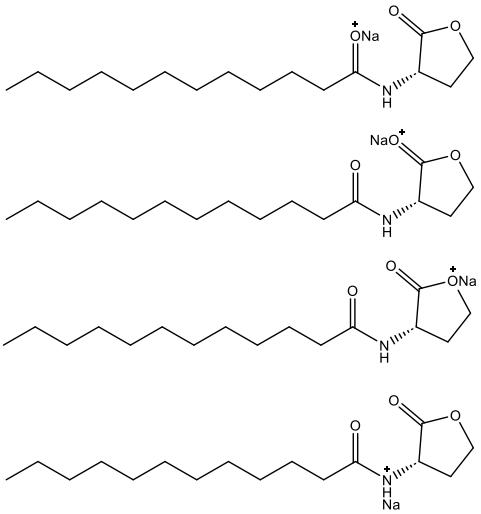

Figure 26: Structures of C12-HSL sodium pseudomolecular ions (m/z 306) with different possible placements for the charge

Figure 26 illustrates the structure of N-dodecanoyl-L-homoserine lactone ionized with sodium. This structure is the same as the one shown in Figure 19, but ionized with sodium instead of protonated. This will be the precursor ion when performing CID on *m/z* 306, as is done when searching for the sodium ions instead of the protonated molecules.

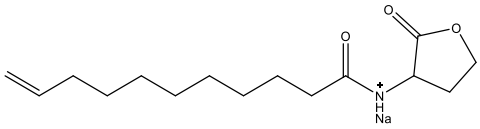

Figure 27: Proposed structures of m/z 290 fragment from C12-HSLNa$^+$ by a remote hydrogen rearrangement

Figure 27 illustrates a fragment (m/z 290) of C12-HSLNa$^+$. The fragmentation reaction which formed this structure was a remote hydrogen rearrangement, where the double bond created ended up on the detected as opposed to on the neutral molecule.

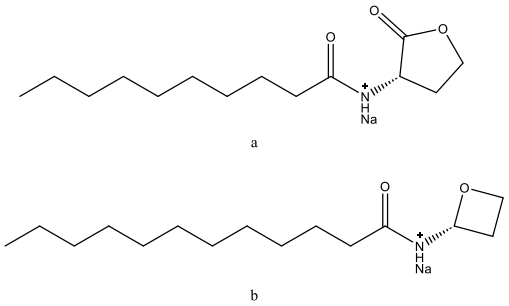

Figure 28: Proposed structures of m/z 256 fragment from C12-HSLNa$^+$ by remote hydrogen rearrangement (a), or by carbon monoxide elimination (b).

Figure 28 illustrates a fragment (m/z 278) of C12-HSLNa$^+$. These fragments arise from remote hydrogen rearrangement (a) and carbon monoxide elimination (b).

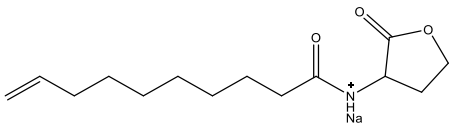

Figure 29: Proposed structures of m/z 276 fragment from C12-HSLNa+ by a remote hydrogen rearrangement.

Figure 29 illustrates a fragment (m/z 276) of C12-HSLNa$^+$. The fragmentation reaction which formed this structure was a remote hydrogen rearrangement, where the double bond created ended up on the detected as opposed to on the neutral molecule.

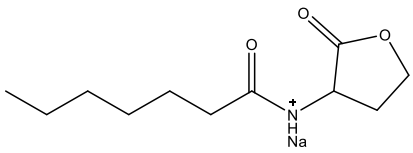

Figure 30: Proposed structures of m/z 2 fragment from C12-HSLNa+ by a remote hydrogen rearrangement

Figure 30 illustrates a fragment (m/z 236) of the C12-HSLNa$^+$. The fragmentation reaction which formed this structure was a remote hydrogen rearrangement, where the double bond created ended up on the neutral molecule as opposed to on the detected ion.

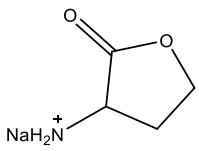

Figure 31: Proposed structures of m/z 124 fragment from C12-HSLNa$^+$ by remote hydrogen rearrangement

Figure 31 illustrates the sodium ion version of the known m/z 102 fragment (*m/z* 124). This structure is a fragment of the structure seen in Figure 26. The fragmentation reaction is remote hydrogen rearrangement.

3.1.4 Fragments of N-tetradecanoyl-L-homoserine lactone

The spectrum of N-tetradecanoyl-L-homoserine lactone can be found in Figure B.VII. and Figure B.VIII. under Appendix B. The presence of N-tetradecanoyl-L-homoserine lactone (C14-HSL) can be determined by finding the peaks *m/z* 312, 158 and 102 in a $M+H^+$ mass spectrum, which correspond to the fragments found in Figures 32, 33 and 34. In addition by finding the peaks *m/z* 334, 304 and 290 in a $M+Na^+$ mass spectrum, which correspond to the fragments found in Figures 35, 36 and 37. The presence of these peaks, as well as the abundance of the ions being similar, describes exactly how the molecules fragment. Seeing as the instrument was set to CID of *m/z* 312 and later *m/z* 334, any peaks that show up in such the spectra will have precursor ions of those masses. If the mass of the precursor ion and the mass of the product ions all match up with the structure of interest one can conclude with the presence of the substance.

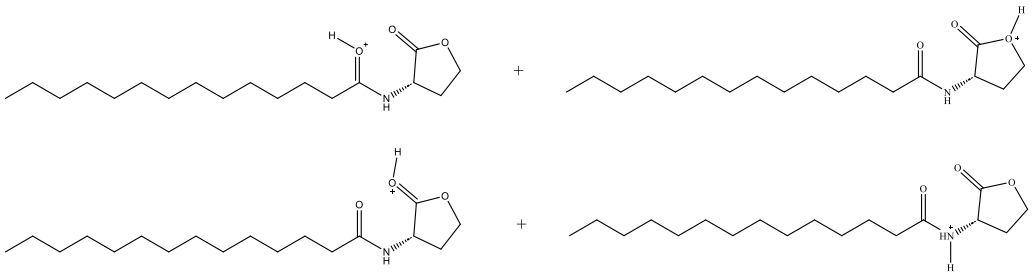

Figure 32: Structures of protonated C14-HSL (m/z 312) with different possible placements of the charge.

Figure 32 illustrates a protonated N-tetradecanoyl-L-homoserine lactone structure. This is the precursor ion when performing CID on *m/z* 312.

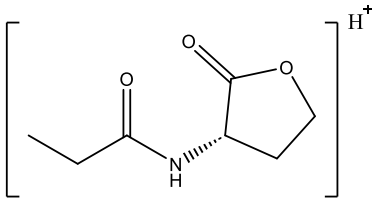

Figure 33: Proposed structure of the fragment with m/z 158 derived from C14-HSL by remote hydrogen rearrangement.

Figure 33 illustrates a fragment from a remote hydrogen rearrangement of N-tetradecanoyl-L-homoserine lactone, the same fragment that arises in fragmentation of N-hexanoyl-L-homoserine lactone (Figure 11)

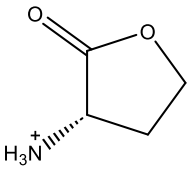

Figure 34: Proposed structures of m/z 102 fragment from protonated C14-HSL by remote hydrogen rearrangement

Figure 34 illustrates another fragment from a remote hydrogen fragmentation of N-hexanoyl-L-homoserine lactone, the previously mentioned 102 fragment which is commonly found in ESI spectra of AHLs.

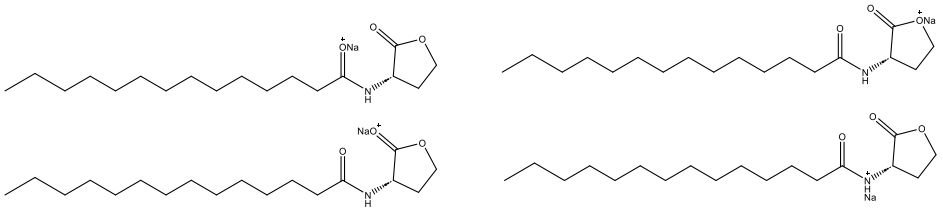

Figure 35: Structures of C14-HSL sodium pseudomolecular ions (m/z 334) with different possible placements for the charge

Figure 35 illustrates the structure of N-tetradecanoyl-L-homoserine lactone ionized with sodium. This structure is the same as the one shown in Figure 29, but ionized with sodium instead of protonated. This will be the precursor ion when performing CID on *m/z* 334, as is done when searching for the sodium ions instead of the protonated molecules mentioned above.

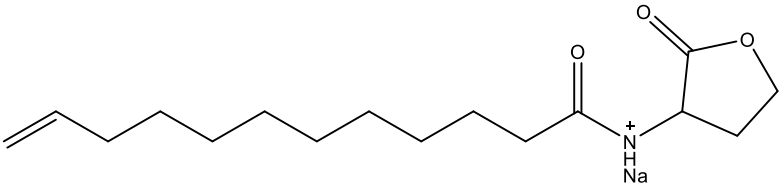

Figure 36: Proposed structure of the fragment with m/z 304 derived from C14-HSL by remote hydrogen rearrangement.

Figure 36 illustrates a remote hydrogen fragmentation (m/z 304) of C14-HSLNa$^+$ where the π bond was formed on the fragment ion as opposed to on the eliminated neutral molecule.

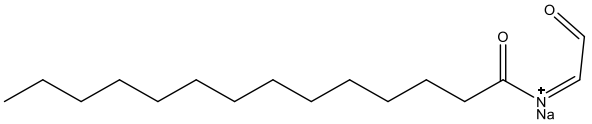

Figure 37: Proposed structure of the fragment with m/z 290 derived from C14-HSLNa+

Figure 37 illustrates a fragment (m/z 290) of C14-HSLNa$^+$ like the fragment of N-hexanoyl-L-homoserine lactone seen in Figure 15.

3.1.5 Fragments of N-(3-oxohexanoyl)-L-homoserine lactone

The spectra of N-(3-oxohexanoyl)-L-homoserine lactone can be found in Figure B.IX. and Figure B.X. under Appendix B. The presence of of N-(3-oxohexanoyl)-L-homoserine lactone (3-O-C6-HSL) can be determined by finding the peaks *m/z* 214, 186 and 170 in a $M+H^+$ mass spectrum, which correspond to the fragments found in Figures 38, 39 and 40. In addition by finding the peaks *m/z* 236, 150 and 124 in a M+Na mass spectrum, which correspond to the fragments found in Figures 41, 42 and 43. The presence of these peaks, as well as the abundance of the ions being similar, describes exactly how the molecules fragment. Seeing as the instrument was set to CID of *m/z* 214 and later *m/z* 226, any peaks that show up in such the spectra will have precursor ions of those masses. If the mass of the precursor ion and the mass of the product ions all match up with the structure of interest one can conclude with the presence of the substance.

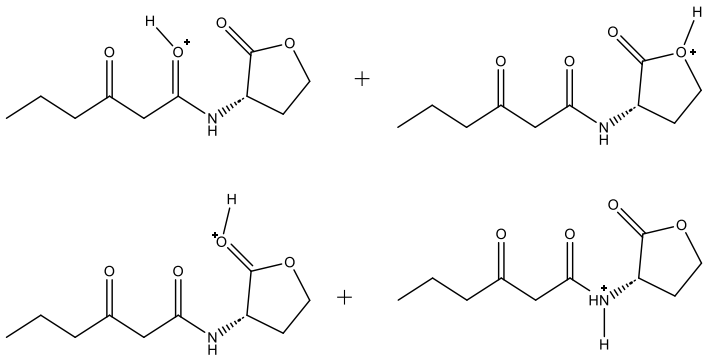

Figure 38: Structures of protonated 3-O-C6-HSL (m/z 214) with different possible placements for the charge.

Figure 38 illustrates a protonated N-(3-oxohexadecanoyl)-L-homoserine lactone ion (*m/z* 214).

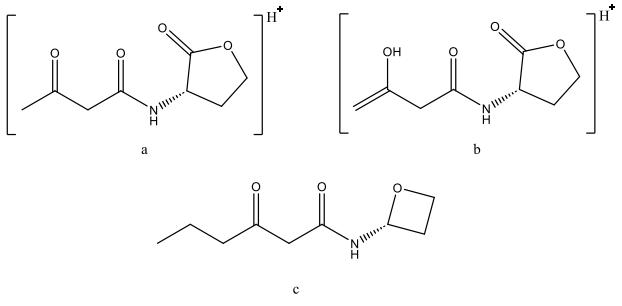

Figure 39: Proposed structures of the fragment with m/z 186 derived from protonated 3-O-C6-HSL through remote hydrogen rearrangement (a, b) and carbon monoxide elimination (c).

Figure 39 illustrates a fragment (m/z 186) of protonated 3-O-C6-HSL. The fragmentation reactions are remote hydrogen rearrangements (a, b) and a carbon monoxide elimination (c).

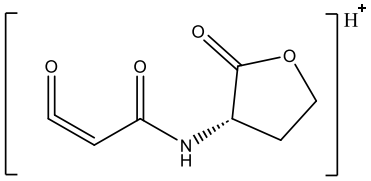

Figure 40: Proposed structures of the fragment with m/z 170 derived from protonated 3-O-C6-HSL through remote hydrogen rearrangement.

Figure 40 illustrates a fragment (*m/z* 170) from a remote hydrogen rearrangement from protonated 3-O-C6-HSL, where the new π bond was formed on the fragment ion as opposed to on the eliminated neutral molecule.

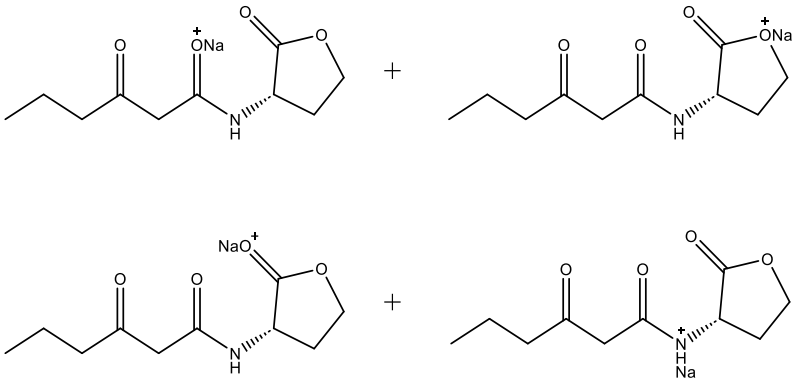

Figure 41: Structures of protonated 3-O-C6-HSLNa$^+$ (m/z 236) with different possible placements for the charge.

Figure 41 illustrates the structure of N-(3-oxohexanoyl)-L-homoserine lactone ionized with sodium. This structure is the same as the one shown in Figure 39 but ionized with sodium instead of protonated. This will be the precursor ion when performing CID on *m/z* 236, as is done when searching for the sodium ions instead of the protonated molecules.

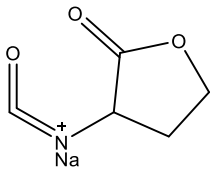

Figure 42: Proposed structures of the fragment (m/z 150) derived from 3-O-C6-HSLNa$^+$ through remote hydrogen rearrangement.

Figure 42 illustrates a fragment (*m/z* 150) from a remote hydrogen rearrangement of 3-O-C6-HSLNa$^+$ where the new π bond was formed on the fragment ion as opposed to on the eliminated neutral molecule.

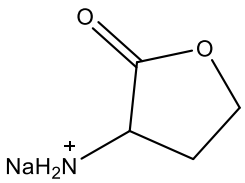

Figure 43: Proposed structures of m/z 124 fragment derived from 3-O-C6-HSLNa+ by remote hydrogen rearrangement.

Figure 43 illustrates another fragment (m/z 124) from a remote hydrogen fragmentation of 3-O-C6-HSLNa$^+$. This is the previously mentioned 102 fragment which is commonly found in ESI spectra of AHLs, ionized with sodium. The fragmentation reaction is a remote hydrogen rearrangement.

3.1.6 N-(3-oxododecanoyl)-L-homoserine lactone

The spectra of N-(3-oxododecanoyl)-L-homoserine lactone can be found in Figure B.XI. and Figure B.XII. under Appendix B. The presence N-(3-oxododecanoyl)-L-homoserine lactone (3-OC12-HSL) can be determined by finding the peaks *m/z* 298, 284 and 254 in a M+H$^+$ mass spectrum, which correspond to the fragments found in Figures 44, 45 and 46. In addition by finding the peaks *m/z* 320, 150 and 124 in a M+Na$^+$ mass spectrum, which correspond to the fragments found in Figures 47, 48 and 49. The presence of these peaks, as well as the abundance of the ions being similar, describes exactly how the molecules fragment. Seeing as the instrument was set to CID of *m/z* 214 and later *m/z* 226, any peaks that show up in such the spectra will have precursor ions of those masses. If the mass of the precursor ion and the mass of the product ions all match up with the structure of interest one can conclude with the presence of the substance.

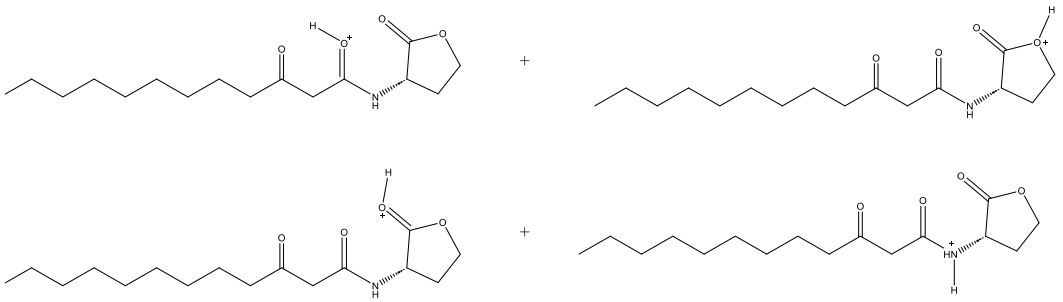

Figure 44: Structures of protonated 3-O-C12-HSL (m/z 298) with different possible placements of the charge

Figure 44 illustrates a protonated N-(3-oxododecanoyl)-L-homoserine lactone ion (*m/z* 298). This is the precursor ion when performing CID on *m/z* 298.

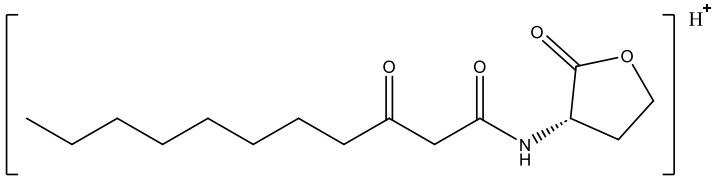

Figure 45: Proposed structures of a fragment (m/z 284) derived from protonated 3-O-C12-HSL by remote hydrogen rearrangement.

Figure 45 illustrates a fragment (m/z 284) of protonated 3-O-C12-HSL. The fragmentation reaction which formed this structure was a remote hydrogen rearrangement, where the double bond created ended up on the neutral molecule as opposed to on the detected ion.

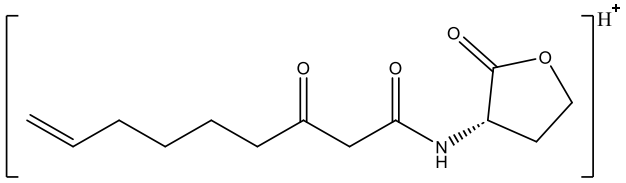

Figure 46: Proposed structures of a fragment (m/z 254) derived from protonated 3-O-C12-HSL by remote hydrogen rearrangement.

Figure 46 illustrates a fragment (m/z 254) of protonated 3-O-C12-HSL. The fragmentation reaction which formed this structure was a remote hydrogen rearrangement, where the double bond created ended up on the detected ion as opposed to on the neutral fragment.

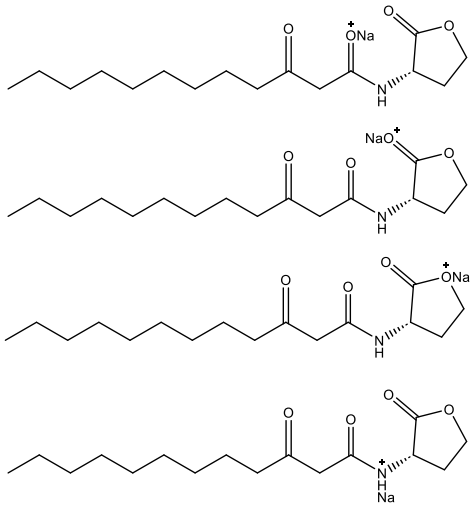

Figure 47: Structures of 3-O-C12-HSLNa$^+$ (m/z 320) with different possible placements of the charge

Figure 47 illustrates the structure of N-(3-oxododecanoyl)-L-homoserine lactone ionized with sodium (*m/z* 320. This will be the precursor ion when performing CID on *m/z* 320, as is done when searching for the sodium ions instead of the protonated molecules.

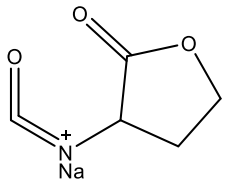

Figure 48: Proposed structures of a fragment (m/z 150) derived from 3-O-C12-HSLNa+ by remote hydrogen rearrangement.

Figure 48 illustrates a fragment (*m/z* 150) from a remote hydrogen rearrangement the structure seen in Figure 47 where the new π bond was formed on the fragment ion as opposed to on the eliminated neutral molecule. This structure is identical to the one seen in Figure 39.

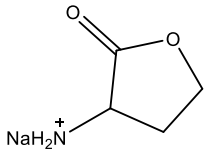

Figure 49: Proposed structures of a fragment (m/z 124) derived from 3-O-C12-HSLNa+ by remote hydrogen rearrangement.

Figure 49 illustrates another fragment (m/z 124) from a remote hydrogen fragmentation of the structure shown in Figure 47. This is the previously mentioned 102 fragment which is commonly found in ESI spectra of AHLs, ionized with sodium. The fragmentation reaction is a remote hydrogen rearrangement. This structure is identical to the one seen in Figure 40.

3.2 Quantitative results

3.2.1 Practical

The optimal collision energy was determined to be 10 eV. The method calls for a several solutions with known concentrations of all the AHLs, here concentrations of 2.5 µg/mL, 5.0 µg/mL, 7.5 µg/mL and 0.01 µg/mL were used.

The MS software set up calls for CID search for all the individual M+1 and M+23 masses listed in Table 2 found in chapter 2.1.2. for 0.3 minutes each and switching out the solution for one with a higher concentration before the instrument started a new round of searches. This method is described in appendix A.III. When the two intensities were observed for a certain value of M, the next step is relating those intensities to the concentration of the corresponding molecule through the standard curve made for this molecule.

3.2.2 Statistical interpretation

The idea was to create a table relating known concentrations to absolute intensity of the pseudomolecular ions detected by the instrument.

The estimated parameters of the regression models can be found using RStudio, though any program with similar capabilities should be applicable. Using the program where the regression models are identified, one can conclude an interval in which the concentration of any sample with known intensities for M+1 and M+23 at a certain collision energy should be identified with a certain level of confidence.

Appendix C illustrates a general code in R studio for estimating the β values, where the summary input grants the β values, alongside a statistical interpretation that speaks on the certainty of the numbers. One can from there on out use the equation like any other standard curve and find the value of y when x_1 and x_2 are known.

3.2.3 Results from an incomplete method

Getting valuable results proved difficult in practice, Theoretically, a relationship between the abundance of pseudomolecular ions (M+1 and M+23) and their concentration should exist and be identifiable.

The suggested input for creating of standard curves are shown in Appendix C.I. The method needs to be applied individually to all values of M, which in the case of this project is six, as

Appendix C.I suggests. Appendix A.II illustrates the table of results used to generate the regression model.

Appendix C.II illustrates the output from R and Table 4 illustrates the β values and the R^2 value found in this output, whereas more information can be found in Appendix C.II.

Table 4: R output values β_1, β_2 and adjusted R^2 for all six analytes

Structure	β_1	β_2	Adjusted R^2
C4-HSL	$-3.641*10^{-8}$	$1.098*10^{-7}$	0.836
C6-HSL	$4.641*10^{-7}$	$4.951*10^{-9}$	0.4773
C12-HSL	$3.314*10^{-7}$	$-3.464*10^{-8}$	0.9854
C14-HSL	$-2.451*10^{-9}$	$2.658*10^{-8}$	0.9724
3-O-C6-HSL	$6.941*10^{-8}$	$1.064*10^{-8}$	0.975
3-O-C12-HSL	$-1.043*10^{-9}$	$6.145*10^{-8}$	0.9136

Negative β-values were not expected, as this suggests a decrease in detected ions with an increase in concentration. The only numbers that, based on Table 4, show usable results, are the values from analysis of C12-HSL. The implications of these numbers will be discussed further in this chapter.

C4-HSL

The RStudio output shows the values for β_1 and β_2 in the equation $y = \beta_0 + \beta_1 x_1 + b_2 x_2$, (where y represents the concentration of C4-HSL, x_1 and x_2 represent the abundance of M+1 = 172 and M+23 = 194, respectively, and $\beta_0 = 0$) along with the R^2 value for the models, residuals, residual standard errors, t values and p-values.

The results shown in Appendix C.II show the following relationship.

$$y = -0.00000003641x_1 + 0.0000001098x_2$$

The adjusted R^2 is 0.836, meaning that the model can describe 83.6 % of the variance of Y. The t-values are -0.056 and 1.358, with corresponding p-values of 0.960 and 0.304.

$P(|T| > t_1|\beta_1 = 0) = 0.$ $P(|T| > t_2|\beta_2 = 0) = 0.477$

The p-values are the probabilities of getting the results in question if there was in fact no relationship between the concentration and the abundances. Both p-values are higher than any

useful level of significance, and the results do not show the expected relationship between concentration and abundance of detected ions.

The adjusted R^2 value is relatively high (compared to C6-HSL), but β_1 is supposed to be a positive number. The t-value is highest for β_2, which along with the relatively high adjusted R^2 is an indicator to try another regression model.

```
RegC4Na <- lm(formula = C ~ 0 + Na, data = a1)
summary (RegC4Na)
```

The code stated above removes the protonated ions from the equation. The result yields an adjusted R^2 value of 0.8905, which shows an increase from before. The outcome, though falling short of standards for R^2, are worth mentioning.

C6-HSL

The RStudio output shows the values for β_1 and β_2 in the equation $y = \beta_0 + \beta_1 x_1 + b_2 x_2$, (where y represents the concentration of C6-HSL, x_1 and x_2 represent the abundance of M+1 = 200 and M+23 = 222, respectively, and $\beta_0 = 0$) along with the R^2 value for the models, residuals, residual standard errors, t values and p-values.

The results shown in Appendix C.II show the following relationship.

$$y = 0.0000004641x_1 + 0.000000004951x_2$$

The adjusted R^2 is 0.4773, meaning that the model can only describe 47.73% of the variance of Y. The t-values are 1.249 and 0.811, with corresponding p-values of 0.300 and 0.477.

$$P(|T| > t_1|\beta_1 = 0) = 0.3 \qquad P(|T| > t_2|\beta_2 = 0) = 0.477$$

The p-values are the probabilities of getting the results in question if there was in fact no relationship between the concentration and the abundances. Both p-values are higher than any useful level of significance, and the results therefore do not show the expected relationship between concentration and abundance of detected ions.

In addition, judging by the R^2 value, the model is not a good for the data as it only explains 47.33 % of variance in concentration. Seeing as the theory states that a linear relationship should be identifiable, the problem is assumed to lie elsewhere.

C12-HSL

The RStudio output shows the values for β_1 and β_2 in the equation $y = \beta_0 + \beta_1 x_1 + b_2 x_2$, (where y represents the concentration of C12-HSL, x_1 and x_2 represent the abundance of M+1 = 284 and M+23 = 306, respectively, and $\beta_0 = 0$) along with the R^2 value for the models, residuals, residual standard errors, t values and p-values.

The results shown in Appendix C.II for show the following relationship.

$$y = 0.0000003314x_1 - 0.00000003464x_2$$

The adjusted R^2 is 0.9854, meaning that the model can describe 98.54% of the variance of Y. The t-values are 11.859 and -6.685, with corresponding p-values of 0.00129 and 0.00683.

$P(|T| > t_1|\beta_1 = 0) = 0.00129 \qquad P(|T| > t_2|\beta_2 = 0) = 0.00683$

The p-values are the probabilities of getting the results in question if there was in fact no relationship between the concentration and the abundances. Both p-values are lower than any most used levels of significance and do show a relationship between abundance and concentration. However, β_2 is negative and the model therefore does not describe the relationship and is not useful in determining concentration. The regression model does describe the data quite well, and removal of any results only generates a less fit model. Just because the data can form a line, that does not mean that the line in question describes the actual relationship between abundance and concentration, or that it would be useful in quantification of C12-HSL.

C14-HSL

The RStudio output shows the values for β_1 and β_2 in the equation $y = \beta_0 + \beta_1 x_1 + b_2 x_2$, (where y represents the concentration of C14-HSL, x_1 and x_2 represent the abundance of M+1 = 312 and M+23 = 334, respectively, and $\beta_0 = 0$) along with the R^2 value for the models, residuals, residual standard errors, t values and p-values.

The results shown in Appendix C.II for show the following relationship.

$$y = -0.000000002451x_1 + 0.00000002658x_2$$

The adjusted R^2 is 0.9724, meaning that the model can describe 97.24% of the variance of Y. The t-values are -0,027 and 1.588, with corresponding p-values of 0.00129 and 0.00683.

$P(|T| > t_1|\beta_1 = 0) = 0.980 \;\; P(|T| > t_2|\beta_2 = 0) = 0.211$

The p-values are the probabilities of getting the results in question if there was in fact no relationship between the concentration and the abundances. Both p-values are higher than any useful level of significance and don't show a relationship between abundance and concentration. However, R^2 is quite high, but that can be explained by a lack of overall variance in x_1 and x_2. The numbers found in table … alone show that a useful curve could not be created.

3-OC6-HSL

The RStudio output shows the values for β_1 and β_2 in the equation $y = \beta_0 + \beta_1 x_1 + b_2 x_2$, (where y represents the concentration of 3-O-C6-HSL, x_1 and x_2 represent the abundance of M+1 = 214 and M+23 = 236, respectively, and $\beta_0 = 0$) along with the R^2 value for the models, residuals, residual standard errors, t values and p-values.

The results shown in Appendix C.II for show the following relationship.

$$y = 0.00000006941x_1 + 0.00000001064x_2$$

The adjusted R^2 is 0.975, meaning that the model can describe 97.5% of the variance of Y. The t-values are 0.820 and 9.271, with corresponding p-values of 0.47235 and 0.00266.

$$P(|T| > t_1|\beta_1 = 0) = 0.47235 \qquad P(|T| > t_2|\beta_2 = 0) = 0.00266$$

The p-values are the probabilities of getting the results in question if there was in fact no relationship between the concentration and the abundances. 0.0026 is lower than most logical levels of significance, which along with the high adjusted R^2 is an indicator to try another regression model.

```
Reg3OC6Na <- lm(formula = C ~ 0 + Na, data = a5)
summary (Reg3OC6Na)
```

The code stated above removes the protonated ions from the equation. The result yields an adjusted R^2 value of 0.977, which shows an increase from before. The t-value is 14.61 and the p-value for β is 0.000128. By studying the numbers, one can see there is a steady increase in abundance as concentration increases. This model might therefore be usable.

3-OC12-HSL

The RStudio output shows the values for β_1 and β_2 in the equation $y = \beta_0 + \beta_1 x_1 + b_2 x_2$, (where y represents the concentration of 3-O-C12-HSL, x_1 and x_2 represent the abundance of M+1 = 298 and M+23 = 320, respectively, and $\beta_0 = 0$) along with the R^2 value for the models, residuals, residual standard errors, t values and p-values.

The results shown in Appendix C.II for show the following relationship.

$$y = -0.000000001043x_1 + 0.000000006145x_2$$

The adjusted R^2 is 0.9136, meaning that the model can describe 91.36 % of the variance of Y. The t-values are -0.152 and 6.375, with corresponding p-values of 0.88885 and 0.00781.

$$P(|T| > t_1|\beta_1 = 0) = 0.88885 \qquad P(|T| > t_2|\beta_2 = 0) = 0.00781$$

The p-values are the probabilities of getting the results in question if there was in fact no relationship between the concentration and the abundances. 0.00781 is lower than most levels of significance, which along with the high adjusted R^2 is an indicator to try another regression model.

```
Reg3OC12Na <- lm(formula = C ~ 0 + Na, data = a6)
summary (Reg3OC12Na)
```

The code stated above removes the protonated ions from the equation. The result yields an adjusted R^2 value of 0.947, which shows an increase from before. The t-value is 8.517 and the p-value for β is 0.00104. By studying the numbers, one can see there is a relatively steady increase in abundance as concentration increases. This model might therefore be usable.

Further discussion

The models was only made with one sample. However, the values listed in the tables in Appendix C.II. are the average abundance of ions detected by the instrument over 0.3 minutes from the same sample. A better fit may have been achieved by using more data. If not, one could conclude that the method was not fit for the task of identifying a relationship between the concentration and abundance.

If the models proved to be a good fit for the data, one could observe values for M+1 and M+23, put them directly into the equations as values for x_1 and x_2, and receive values for y determining the concentrations of the AHLs. If it were preferable, one could create confidence intervals to claim with a given certainty that the concentration lies between A mg/mL and B mg/mL using the following R code found below.

```
predict(RegX, data.frame(H=A[M+1]obs, Na=A[M+23]obs), interval='confidence',
level=1-α)
```

The code above requires the code found in Appendix C.II to be ran previously, as the regression model labelled as “RegX” needs to exist in RStudio’s dataset. The code could be applied to all the models, by replacing “RegX” the regression in question. It also requires the

users input of the observed abundances, $A[M+1]_{obs}$ and $A[M+23]_{obs}$, as well as the level of significance α (if not specified, α=0.05).

If done correctly, one can in theory get several pieces of information from this method that uses standard curve via multiple linear regression, but it is however tedious work. Xcalibur shows the abundance of ions, but they need to be manually put into a spreadsheet (Excel, in this case) alongside their respective concentrations and imported into RStudio before the results can be processed. That workload could probably be minimized by someone who is more proficient in programming than the author.

4 Conclusion and further work

This thesis involved an aim to primarily identify the presence of six specific AHLs using direct infusion ESI-MS. There was also an attempt to quantify these substances by direct infusing ESI-MS by creating a linear regression model that would act as standard curve describing the relationship between the abundances of detected ions and the concentration of the AHLs, which did not yield useful results.

Direct infusion with a Hamilton syringe requires manual switching between solutions, while using an autosampler would automate that task. The identification requires manual interpretation of the spectra, and the quantification requires manual transfer of data to spreadsheets. These aspects make the work time consuming and ineffective. Employing the commonly used HPLC-MS technique would be a far more effective approach if one wishes to perform the tasks of identification and quantification.

The use of a linear standard curve with two explanatory variables proved to be difficult. If one wishes to achieve the quantification by utilizing the multiple linear regression model described, more reliable results could possibly be obtained by using 3-5 parallels when creating the curves. This action would result in several times more data that would need to be manually written into the spreadsheets. An automatization of this step would be necessary at that point. A non-linear relationship might exist between the abundances and the concentration. Such a relationship was not hypothecated and therefore not studied. This could be studied further.

6 References

(1) Nealson, K. H.; Platt, T.; Hastings, J. W. Cellular control of the synthesis and activity of the bacterial luminescent system. *Journal of bacteriology* **1970**, *104* (1), 313-322.

(2) Fuqua, W. C.; Winans, S. C.; Greenberg, E. P. Quorum sensing in bacteria: the LuxR-LuxI family of cell density-responsive transcriptional regulators. *Journal of bacteriology* **1994**, *176* (2), 269-275.

(3) Eberhard, A.; Burlingame, A. L.; Eberhard, C.; Kenyon, G. L.; Nealson, K. H.; Oppenheimer, N. J. Structural identification of autoinducer of Photobacterium fischeri luciferase. *Biochemistry* **1981**, *20* (9), 2444-2449. DOI: 10.1021/bi00512a013.

(4) Boo, A.; Ledesma Amaro, R.; Stan, G.-B. Quorum sensing in synthetic biology: A review. *Current Opinion in Systems Biology* **2021**, *28*, 100378. DOI: 10.1016/j.coisb.2021.100378.

(5) Rodrigues, A. M. S.; Lami, R.; Escoubeyrou, K.; Intertaglia, L.; Mazurek, C.; Doberva, M.; Pérez-Ferrer, P.; Stien, D. Straightforward N-Acyl Homoserine Lactone Discovery and Annotation by LC–MS/MS-based Molecular Networking. *Journal of Proteome Research* **2022**, *21* (3), 635-642. DOI: 10.1021/acs.jproteome.1c00849.

(6) Kostylev, M.; Kim, D. Y.; Smalley, N. E.; Salukhe, I.; Greenberg, E. P.; Dandekar, A. A. Evolution of the Pseudomonas aeruginosa quorum-sensing hierarchy. *Proceedings of the National Academy of Sciences* **2019**, *116* (14), 7027-7032. DOI: 10.1073/pnas.1819796116.

(7) Dewick, P. M. *Medicinal Natural Products: A Biosynthetic Approach*; John Wiley and Sons, 2009.

(8) Huber, T. D.; Johnson, B. R.; Zhang, J.; Thorson, J. S. AdoMet analog synthesis and utilization: current state of the art. *Current Opinion in Biotechnology* **2016**, *42*, 189-197. DOI: 10.1016/j.copbio.2016.07.005.

(9) Scoffone, V. C.; Chiarelli, L. R.; Makarov, V.; Brackman, G.; Israyilova, A.; Azzalin, A.; Forneris, F.; Riabova, O.; Savina, S.; Coenye, T.; et al. Discovery of new diketopiperazines inhibiting Burkholderia cenocepacia quorum sensing in vitro and in vivo. *Scientific Reports* **2016**, *6* (1), 32487. DOI: 10.1038/srep32487.

(10) Sufrin, J.; Finckbeiner, S.; Oliver, C. Marine-Derived Metabolites of S-Adenosylmethionine as Templates for New Anti-Infectives. *Marine Drugs* **2009**, *7* (3), 401-434. DOI: 10.3390/md7030401.

(11) Demarque, D. P.; Crotti, A. E. M.; Vessecchi, R.; Lopes, J. L. C.; Lopes, N. P. Fragmentation reactions using electrospray ionization mass spectrometry: an important tool for the structural elucidation and characterization of synthetic and natural products. *Natural Product Reports* **2016**, *33* (3), 432-455. DOI: 10.1039/c5np00073d.

(12) de Hoffmann, E.; Strooband, V. *Mass Spectrometry: Principles and Applications*; John Wiley & Sons, 2007.

(13) Banerjee, S.; Mazumdar, S. Electrospray Ionization Mass Spectrometry: A Technique to Access the Information beyond the Molecular Weight of the Analyte. *International Journal of Analytical Chemistry* **2012**, *2012*, 1-40. DOI: 10.1155/2012/282574.

(14) Schwartz, J. C.; Senko, M. W.; Syka, J. E. P. A two-dimensional quadrupole ion trap mass spectrometer. *Journal of the American Society for Mass Spectrometry* **2002**, *13* (6), 659-669. DOI: https://doi.org/10.1016/S1044-0305(02)00384-7.

(15) Hager, J. W. A new linear ion trap mass spectrometer. **2002**, *16* (6), 512. DOI: 10.1002/rcm.607.abs.

(16) Patel, N. M.; Moore, J. D.; Blackwell, H. E.; Amador-Noguez, D. Identification of Unanticipated and Novel N-Acyl L-Homoserine Lactones (AHLs) Using a Sensitive Non-Targeted LC-MS/MS Method. *PLOS ONE* **2016**, *11* (10), e0163469. DOI: 10.1371/journal.pone.0163469.

(17) Ortori, C. A.; Dubern, J.-F.; Chhabra, S. R.; Cámara, M.; Hardie, K.; Williams, P.; Barrett, D. A. Simultaneous quantitative profiling of N-acyl-l-homoserine lactone and 2-alkyl-4(1H)-quinolone families of quorum-sensing signaling molecules using LC-MS/MS. *Analytical and Bioanalytical Chemistry* **2011**, *399* (2), 839-850. DOI: 10.1007/s00216-010-4341-0.

Appendix

Appendix A – Tables

A.I.

Tabell A.I.: The general program for determining optimal collision energies.

Time start (min)	Time end (min)	CI (eV)	*m/z*
0	0.3	5	M+1
0.4	0.7	10	M+1
0.8	1.1	15	M+1
1.2	1.5	20	M+1
1.6	1.9	25	M+1
2	2.3	30	M+1
2.4	2.7	35	M+1
2.8	3.1	40	M+1
3.2	3.5	45	M+1
3.6	3.9	50	M+1
4	4.3	55	M+1
4.4	4.7	60	M+1
4.8	5.1	65	M+1
5.2	5.5	70	M+1
5.6	5.9	75	M+1
6	6.3	80	M+1
6.4	6.7	85	M+1
6.8	7.1	90	M+1
7.2	7.5	95	M+1
7.6	7.9	100	M+1
8	8.3	5	M+23
8.4	8.7	10	M+23
8.8	9.1	15	M+23
9.2	9.5	20	M+23
9.6	9.9	25	M+23
10	10.3	30	M+23
10.4	10.7	35	M+23
10.8	11.1	40	M+23
11.2	11.5	45	M+23
11.6	11.9	50	M+23
12	12.3	55	M+23
12.4	12.7	60	M+23
12.8	13.1	65	M+23
13.2	13.5	70	M+23
13.6	13.9	75	M+23
14	14.3	80	M+23
14.4	14.7	85	M+23
14.8	15.1	90	M+23
15.2	15.5	95	M+23
15.6	15.9	100	M+23

A.II.

C4.HSL.xlsx

Table A.II.I: The results used for creating the regression model describing the relationship between the abundances of ions and the concentration of C4-HSL

C	H	Na
0	2860	974
0.0025	4741	32547
0.005	6639	59860
0.0075	6115	50819

C6HSL.xlsx

Table A.II.II: The results used for creating the regression model describing the relationship between the abundances of ions and the concentration of C6-HSL

C	H	Na
0	1451	835
0.0025	8424	51633
0.005	9496	79433
0.0075	9148	955327
0.01	3645	202735

C12HSL.xlsx

Table A.II.III: The results used for creating the regression model describing the relationship between the abundances of ions and the concentration of C12-HSL

C	H	Na
0	948	1165
0.0025	20663	116562
0.005	28207	109898
0.0075	36716	150803
0.001	24868	210534

C14HSL.xlsx

Table A.II.IV: The results used for creating the regression model describing the relationship between the abundances of ions and the concentration of C14-HSL

C	H	Na
0	1492	984
0.0025	31773	147883
0.005	30096	152848
0.0075	55282	270053
0.01	63492	389649

3OC6HSL.xlsx

Table A.II.V: The results used for creating the regression model describing the relationship between the abundances of ions and the concentration of 3-O-C6-HSL

C	H	Na
0	3209	981
0.0025	9644	276314
0.005	10179	290014
0.0075	6112	687081
0.01	4503	898094

3OC12HSL.xlsx

Table A.II.VI: The results used for creating the regression model describing the relationship between the abundances of ions and the concentration of 3-O-C12-HSL

C	H	Na
0	1223	707
0.0025	291257	488392
0.005	39850	494636
0.0075	47958	916906
0.01	80647	1871613

A.III.

Table A.III: The program for finding the relationship between the abundances of ions and the concentrations of AHLs. (results shown in chapter A.II)

Time start (min)	CI (eV)	m/z	Concentration	Analyte
0	10	172.2	0	C4-HSL H
0.3	10	194.2	0	C4-HSL Na
0.6	10	200.2	0	C6-HSL H
0.9	10	222.2	0	C6-HSL Na
1.2	10	284.4	0	C12-HSL H
1.5	10	306.4	0	C12-HSL Na
1.8	10	312.5	0	C14-HSL H
2.1	10	334.5	0	C14-HSL Na
2.4	10	214.2	0	3-O-C6-HSL H
2.7	10	236.2	0	3-O-C6-HSL Na
3	10	298.4	0	3-O-C12-HSL H
3.3	10	320.4	0	3-O-C12-HSL Na
3.6	10	500	Switch	
7	10	172.2	0.0025	C4-HSL H
7.3	10	194.2	0.0025	C4-HSL Na
7.6	10	200.2	0.0025	C6-HSL H
7.9	10	222.2	0.0025	C6-HSL Na
8.2	10	284.4	0.0025	C12-HSL H
8.5	10	306.4	0.0025	C12-HSL Na
8.8	10	312.5	0.0025	C14-HSL H
9.1	10	334.5	0.0025	C14-HSL Na
9.4	10	214.2	0.0025	3-O-C6-HSL H
9.7	10	236.2	0.0025	3-O-C6-HSL Na
10	10	298.4	0.0025	3-O-C12-HSL H
10.3	10	320.4	0.0025	3-O-C12-HSL Na
10.6	10	500	Switch	
14	10	172.2	0.005	C4-HSL H
14.3	10	194.2	0.005	C4-HSL Na
14.6	10	200.2	0.005	C6-HSL H
14.9	10	222.2	0.005	C6-HSL Na
15.2	10	284.4	0.005	C12-HSL H

15.5	10	306.4	0.005	C12-HSL Na
15.8	10	312.5	0.005	C14-HSL H
16.1	10	334.5	0.005	C14-HSL Na
16.4	10	214.2	0.005	3-O-C6-HSL H
16.7	10	236.2	0.005	3-O-C6-HSL Na
17	10	298.4	0.005	3-O-C12-HSL H
17.3	10	320.4	0.005	3-O-C12-HSL Na
17.6	10	500	Switch	
21	10	172.2	0.0075	C4-HSL H
21.3	10	194.2	0.0075	C4-HSL Na
21.6	10	200.2	0.0075	C6-HSL H
21.9	10	222.2	0.0075	C6-HSL Na
22.2	10	284.4	0.0075	C12-HSL H
22.5	10	306.4	0.0075	C12-HSL Na
22.8	10	312.5	0.0075	C14-HSL H
23.1	10	334.5	0.0075	C14-HSL Na
23.4	10	214.2	0.0075	3-O-C6-HSL H
23.7	10	236.2	0.0075	3-O-C6-HSL Na
24	10	298.4	0.0075	3-O-C12-HSL H
24.3	10	320.4	0.0075	3-O-C12-HSL Na
24.6	10	500	Switch	
28	10	172.2	0.001	C4-HSL H
28.3	10	194.2	0.001	C4-HSL Na
28.6	10	200.2	0.001	C6-HSL H
28.9	10	222.2	0.001	C6-HSL Na
29.2	10	284.4	0.001	C12-HSL H
29.5	10	306.4	0.001	C12-HSL Na
29.8	10	312.5	0.001	C14-HSL H
30.1	10	334.5	0.001	C14-HSL Na
30.4	10	214.2	0.001	3-O-C6-HSL H
30.7	10	236.2	0.001	3-O-C6-HSL Na
31	10	298.4	0.001	3-O-C12-HSL H
31.3	10	320.4	0.001	3-O-C12-HSL Na

A.IV.

Time start (min)		CI (eV)	m/z	Analyte
0	0.3	25	172.2	C4-HSL H
0.4	0.7	25	194.2	C4-HSL Na
0.8	1.1	25	200.2	C6-HSL H
1.2	1.5	25	222.2	C6-HSL Na
1.6	1.9	25	284.4	C12-HSL H
2	2.3	25	306.4	C12-HSL Na
2.4	2.7	25	312.5	C14-HSL H
2.8	3.1	25	334.5	C14-HSL Na
3.2	3.5	25	214.2	3-O-C6-HSL H
3.6	3.9	25	236.2	3-O-C6-HSL Na
4	4.3	25	298.4	3-O-C12-HSL H
4.4	4.7	25	320.4	3-O-C12-HSL Na

Appendix B - Spectra

B.I.

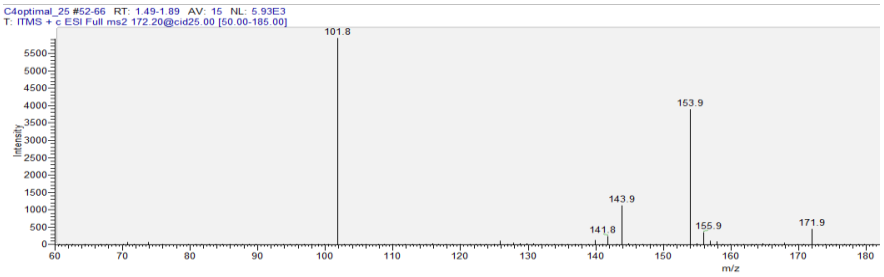

Figure B.I.: The optimal energy for identification for C4-HSL with search for protonated molecular ion was determined to be 25 eV

B.II.

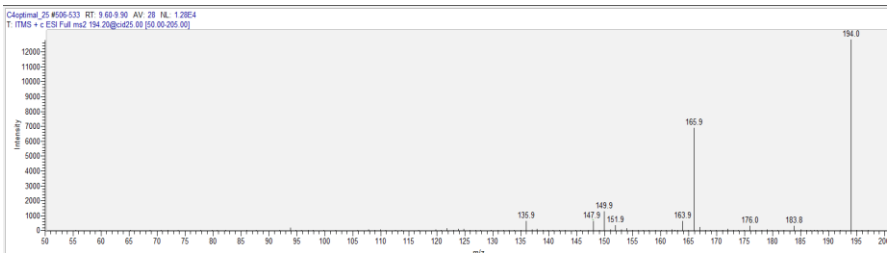

Figure B.II.: The optimal energy for identification of C4-HSL with search for sodium pseudomolecular ion was determined to be 25 eV

B.III.

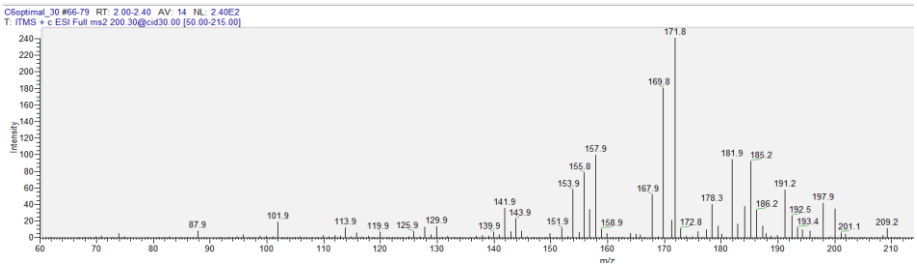

Figure B.III.: The optimal energy of identification for C6-HSL with search for protonated molecular ion was determined to be 30 eV.

B.IV.

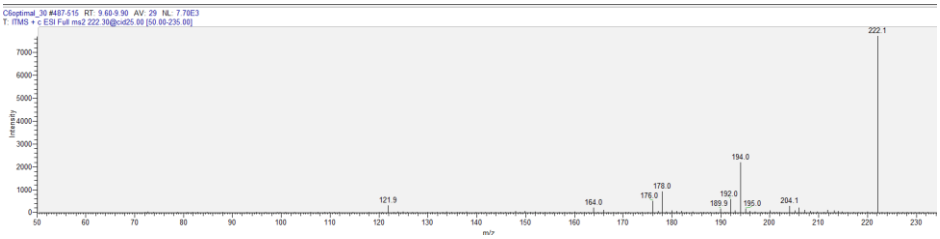

Figure B.IV.: The optimal energy for identification of C6-HSL with search for sodium pseudomolecular ion was determined to be 30 eV

B.V.

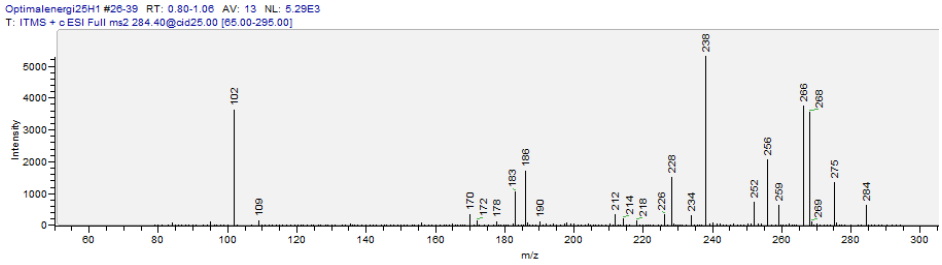

Figure B.V.: The optimal energy for identification of C12-HSL with search for protonated molecular ion was determined to be 25 eV

B.VI.

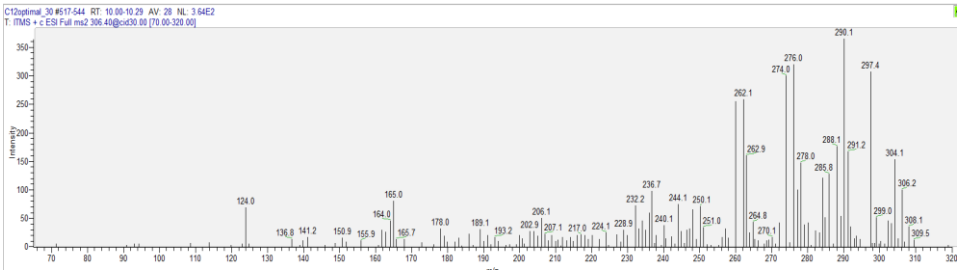

Figure B.VI.: The optimal energy for identification of C6-HSL with search for sodium pseudomolecular ion was determined to be 30 eV

B.VII.

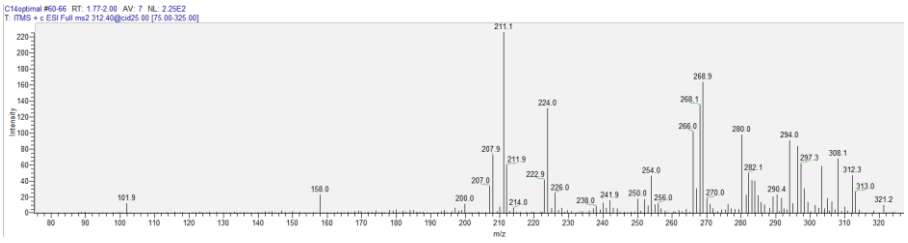

Figure B.VII..: The optimal energy for identification of C14-HSL with search for sodium pseudomolecular ion was determined to be 25 eV

B.VIII.

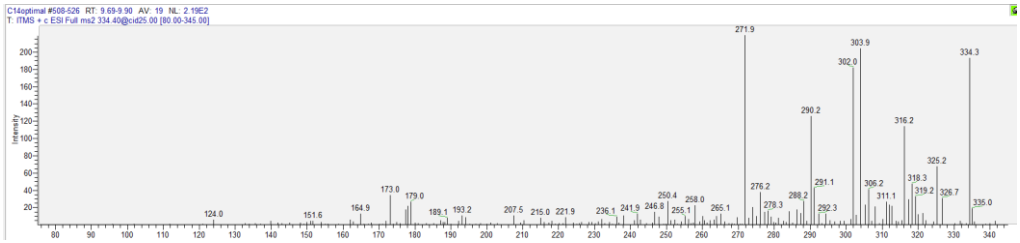

Figure B.VIII.: The optimal energy for identification of C14-HSL with search for protonated molecular ion was determined to be 25 eV

B.IX.

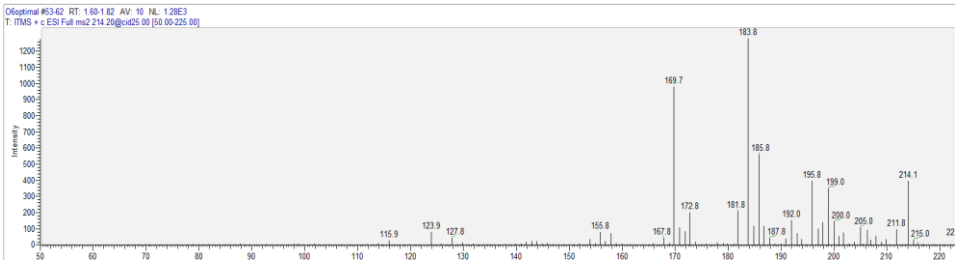

Figure B.IX.: The optimal energy for identification of 3-O-C6-HSL with search for protonated molecular ion was determined to be 25 eV.

B.X.

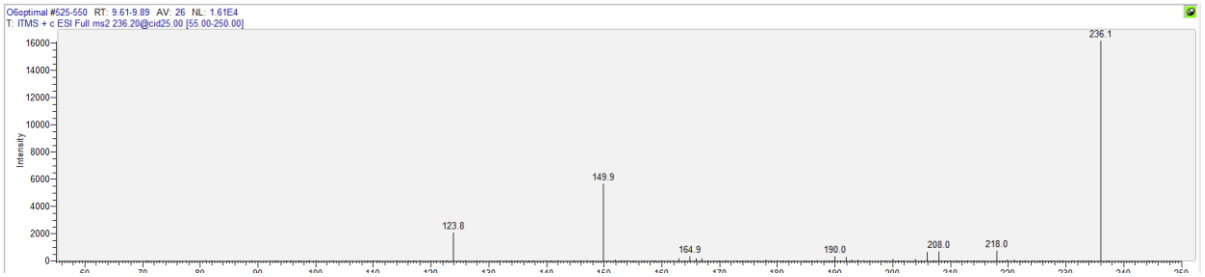

Figure B.X.: The optimal energy for identification of 3-O-C6-HSL with search for protonated molecular ion was determined to be 25 eV

B.XI.

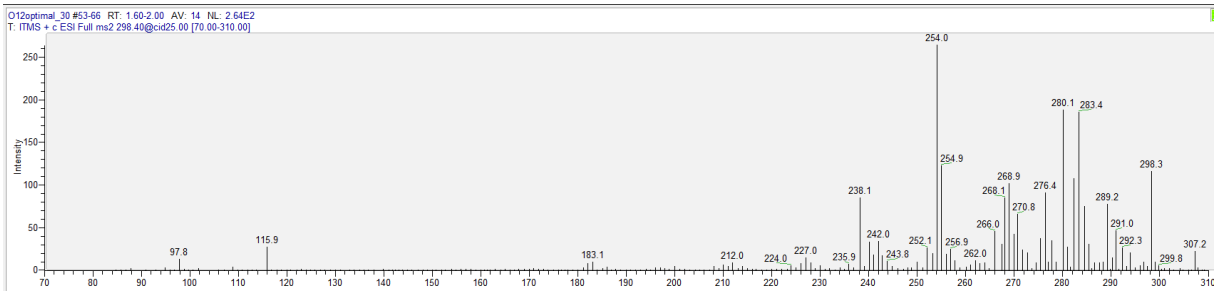

Figure B.XI.: Optimal energy for identification of 3-O-C12-HSL with search for protonated molecular ion was determined to be 30 eV.

B.XII.

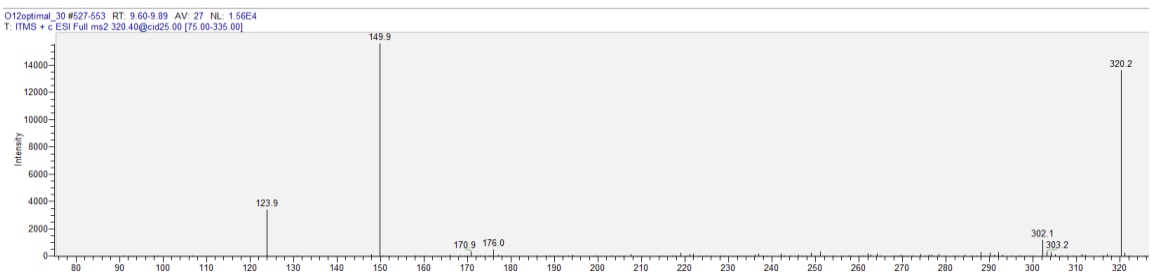

Figure B.XII.: The optimal energy for identification of 3-O-C12-HSL with search for protonated molecular ion was determined to be 25 eV.

Appendix C – Programming

C.I.

```
library(readxl)
a1 <- read_excel("File path C4-HSL results")
a2 <- read_excel("File path C6-HSL results")
a3 <- read_excel("File path C12-HSL results")
a4 <- read_excel("File path C14-HSL results")
a5 <- read_excel("File path 3-O-C6-HSL results")
a6 <- read_excel("File path 3-O-C12-HSL results")

RegC4 <- lm(C~0+H+Na, data=a1)
RegC6 <- lm(C~0+H+Na, data=a2)
RegC12 <- lm(C~0+H+Na, data=a3)
RegC14 <- lm(C~0+H+Na, data=a4)
Reg3OC6<- lm(C~0+H+Na, data=a5)
Reg3OC12<- lm(C~0+H+Na, data=a6)

summary(RegC4)
summary(RegC6)
summary(RegC12)
summary(RegC14)
summary(Reg3OC6)
summary(Reg3OC12)
```

C.II.

```
> summary(RegC4)
Call:
lm(formula = C ~ O + H + Na, data = a1)

Residuals:
         1          2          3          4
-2.816e-06 -9.006e-04 -1.330e-03  2.143e-03

Coefficients:
     Estimate Std. Error t value Pr(>|t|)
H  -3.641e-08  6.490e-07  -0.056    0.960
Na  1.098e-07  8.085e-08   1.358    0.307

Residual standard error: 0.001894 on 2 degrees of freedom
Multiple R-squared:  0.918,    Adjusted R-squared:  0.836
F-statistic:  11.2 on 2 and 2 DF,  p-value: 0.08199

> summary(RegC6)
Call:
lm(formula = C ~ O + H + Na, data = a2)

Residuals:
         1          2          3          4          5
-0.0006776 -0.0016655  0.0001993 -0.0014761  0.0073044

Coefficients:
    Estimate Std. Error t value Pr(>|t|)
H  4.641e-07  3.716e-07   1.249    0.300
Na 4.951e-09  6.109e-09   0.811    0.477

Residual standard error: 0.004427 on 3 degrees of freedom
Multiple R-squared:  0.6864,   Adjusted R-squared:  0.4773
F-statistic: 3.283 on 2 and 3 DF,  p-value: 0.1756

> summary(RegC12)
Call:
lm(formula = C ~ O + H + Na, data = a3)

Residuals:
         1          2          3          4          5
-2.736e-04 -3.086e-04 -5.392e-04  5.586e-04  5.371e-05

Coefficients:
     Estimate Std. Error t value Pr(>|t|)
H   3.314e-07  2.794e-08  11.859  0.00129 **
```

```
Na -3.464e-08  5.182e-09  -6.685  0.00683 **
---
Signif. codes:  0 ‘***’ 0.001 ‘**’ 0.01 ‘*’ 0.05 ‘.’ 0.1 ‘ ’ 1

Residual standard error: 0.0005085 on 3 degrees of freedom
Multiple R-squared:  0.9912,   Adjusted R-squared:  0.9854
F-statistic: 169.6 on 2 and 3 DF,  p-value: 0.0008206

> summary(RegC14)
Call:
lm(formula = C ~ 0 + H + Na, data = a4)

Residuals:
         1          2          3          4          5
-2.251e-05 -1.353e-03  1.011e-03  4.579e-04 -2.006e-04

Coefficients:
     Estimate Std. Error t value Pr(>|t|)
H  -2.451e-09  9.165e-08  -0.027    0.980
Na  2.658e-08  1.674e-08   1.588    0.211

Residual standard error: 0.001017 on 3 degrees of freedom
Multiple R-squared:  0.9835,   Adjusted R-squared:  0.9724
F-statistic: 89.14 on 2 and 3 DF,  p-value: 0.002129

> summary(Reg3OC6)
Call:
lm(formula = C ~ 0 + H + Na, data = a5)

Residuals:
         1          2          3          4          5
-0.0002332 -0.0011095  0.0012077 -0.0002350  0.0001314

Coefficients:
    Estimate Std. Error t value Pr(>|t|)
H  6.941e-08  8.465e-08   0.820  0.47235
Na 1.064e-08  1.148e-09   9.271  0.00266 **
---
Signif. codes:  0 ‘***’ 0.001 ‘**’ 0.01 ‘*’ 0.05 ‘.’ 0.1 ‘ ’ 1

Residual standard error: 0.0009689 on 3 degrees of freedom
Multiple R-squared:  0.985,    Adjusted R-squared:  0.975
F-statistic: 98.37 on 2 and 3 DF,  p-value: 0.001841

> summary(Reg3OC12)
Call:
lm(formula = C ~ 0 + H + Na, data = a6)
```

```
Residuals:
         1          2          3          4          5
-3.065e-06 -1.972e-04  2.002e-03  1.916e-03 -1.416e-03

Coefficients:
     Estimate Std. Error t value Pr(>|t|)
H  -1.043e-09  6.862e-09  -0.152  0.88885
Na  6.145e-09  9.638e-10   6.375  0.00781 **
---
Signif. codes:  0 ‘***’ 0.001 ‘**’ 0.01 ‘*’ 0.05 ‘.’ 0.1 ‘ ’ 1

Residual standard error: 0.0018 on 3 degrees of freedom
Multiple R-squared:  0.9481,   Adjusted R-squared:  0.9136
F-statistic: 27.42 on 2 and 3 DF,  p-value: 0.01181
```

Norges miljø- og biovitenskapelige universitet
Noregs miljø- og biovitskapelege universitet
Norwegian University of Life Sciences

Postboks 5003
NO-1432 Ås
Norway